













# A virtual memory CD8<sup>+</sup> T cell-originated subset causes alopecia areata through innate-like cytotoxicity

Received: 8 June 2022

Accepted: 1 June 2023

Published online: 26 June 2023

 Check for updates

Joon Seok <sup>1,2,9</sup>, Sung-Dong Cho<sup>1,9</sup>, Jeongsoo Lee<sup>1</sup>, Yunseo Choi<sup>1</sup>, Su-Young Kim <sup>2</sup>, Sung-Min Lee<sup>3,4</sup>, Sang-Hoon Kim <sup>5</sup>, Seongju Jeong <sup>1</sup>, Minwoo Jeon<sup>1</sup>, Hoyoung Lee<sup>5</sup>, A. Reum Kim<sup>1</sup>, Baekgyu Choi<sup>3</sup>, Sang-Jun Ha <sup>6</sup>, Inkyung Jung <sup>3</sup>, Ki-Jun Yoon<sup>3,4</sup>, Jong-Eun Park <sup>1</sup>, Jong Hoon Kim <sup>7</sup>, Beom Joon Kim<sup>2</sup>, Eui-Cheol Shin <sup>1,5</sup>  & Su-Hyung Park <sup>1,8</sup> 

Virtual memory T (T<sub>VM</sub>) cells are a T cell subtype with a memory phenotype but no prior exposure to foreign antigen. Although T<sub>VM</sub> cells have antiviral and antibacterial functions, whether these cells can be pathogenic effectors of inflammatory disease is unclear. Here we identified a T<sub>VM</sub> cell-originated CD44<sup>super-high(s-hi)</sup>CD49d<sup>lo</sup> CD8<sup>+</sup> T cell subset with features of tissue residency. These cells are transcriptionally, phenotypically and functionally distinct from conventional CD8<sup>+</sup> T<sub>VM</sub> cells and can cause alopecia areata. Mechanistically, CD44<sup>s-hi</sup>CD49d<sup>lo</sup> CD8<sup>+</sup> T cells could be induced from conventional T<sub>VM</sub> cells by interleukin (IL)-12, IL-15 and IL-18 stimulation. Pathogenic activity of CD44<sup>s-hi</sup>CD49d<sup>lo</sup> CD8<sup>+</sup> T cells was mediated by NKG2D-dependent innate-like cytotoxicity, which was further augmented by IL-15 stimulation and triggered disease onset. Collectively, these data suggest an immunological mechanism through which T<sub>VM</sub> cells can cause chronic inflammatory disease by innate-like cytotoxicity.

Classically, immunological memory is antigen specific. In an unmanipulated host, the majority of CD8<sup>+</sup> T cells have naive phenotypes (T<sub>N</sub> cells), but a substantial population of CD8<sup>+</sup> T cells express phenotypical markers of immunological memory. One such cell population is CD8<sup>+</sup> T<sub>VM</sub> cells, which are characterized by high CD44 expression and low CD49d expression (CD44<sup>hi</sup>CD49d<sup>lo</sup>)<sup>1–3</sup>, and are semi-differentiated but have not been exposed to a foreign antigen, as evidenced by their presence in germ-free mice<sup>4</sup>. Despite being antigenically naive, CD8<sup>+</sup> T<sub>VM</sub> cells are functionally distinct from T<sub>N</sub> cells, being able to more

rapidly induce cytokine production upon T cell antigen receptor (TCR) stimulation and cytokine stimulation<sup>4–7</sup>.

Several studies suggest that CD8<sup>+</sup> T<sub>VM</sub> cells contribute to antiviral, antibacterial, and antitumor immunity<sup>6,8–10</sup>. Mouse studies demonstrate that IL-4 or IL-15 generated during infections can increase the T<sub>VM</sub> cell population<sup>6,8,9</sup>, which can improve antiviral and antibacterial function<sup>8–10</sup>. It has been also suggested that T<sub>VM</sub> cells infiltrate the tumor microenvironment more than T<sub>N</sub> cells<sup>11</sup>, and can mediate tumor cell killing in a TCR-independent manner<sup>12</sup>. Although some studies indicate

<sup>1</sup>Graduate School of Medical Science and Engineering, Korea Advanced Institute of Science and Technology, Daejeon, Republic of Korea. <sup>2</sup>Department of Dermatology, Chung-Ang University Hospital, Chung-Ang University College of Medicine, Seoul, Republic of Korea. <sup>3</sup>Department of Biological Science, Korea Advanced Institute of Science and Technology, Daejeon, Republic of Korea. <sup>4</sup>KAIST Stem Cell Center, Korea Advanced Institute of Science and Technology, Daejeon, Republic of Korea. <sup>5</sup>The Center for Viral Immunology, Korea Virus Research Institute, Institute for Basic Science (IBS), Daejeon, Republic of Korea. <sup>6</sup>Department of Biochemistry, College of Life Science and Biotechnology, Yonsei University, Seoul, Republic of Korea. <sup>7</sup>Department of Dermatology and Cutaneous Biology Research Institute, Gangnam Severance Hospital, Yonsei University College of Medicine, Seoul, Republic of Korea. <sup>8</sup>The Center for Epidemic Preparedness, KAIST Institute, Daejeon, Republic of Korea. <sup>9</sup>These authors contributed equally: Joon Seok, Sung-Dong Cho.

 e-mail: [ecshin@kaist.ac.kr](mailto:ecshin@kaist.ac.kr); [park3@kaist.ac.kr](mailto:park3@kaist.ac.kr)

that the CD8<sup>+</sup> T<sub>VM</sub> cell population has a protective function against pathogens, none have examined the potential pathogenic function of this population in inducing inflammatory diseases. Moreover, the heterogeneity in subpopulations of T<sub>VM</sub> cells and the distinct effector functions of each subset are unclear.

Here, we investigated the pathogenic function of CD8<sup>+</sup> T<sub>VM</sub> cells in alopecia areata (AA), a CD8<sup>+</sup> T cell-mediated chronic inflammatory disease characterized by the rapid onset of hair loss in a sharply defined area<sup>13,14</sup>. Although it has been suggested that cytotoxic CD8<sup>+</sup> T cells have a critical role in initiating AA<sup>14,15</sup>, which CD8<sup>+</sup> T cell subset induces disease pathogenesis is unknown. We identified a distinct CD8<sup>+</sup> T cell population that originates from CD8<sup>+</sup> T<sub>VM</sub> cells, has strong NKG2D-mediated innate-like cytotoxicity and features of tissue residency and can cause the chronic inflammatory disease AA.

## Results

### CD44<sup>hi</sup>CD49d<sup>lo</sup> CD8<sup>+</sup> T cells cause alopecia areata

To investigate the function of T<sub>VM</sub> cells in AA pathogenesis, we measured the frequency of T<sub>VM</sub> cells (CD44<sup>hi</sup>CD49d<sup>lo</sup> CD8<sup>+</sup> T cells) among total CD8<sup>+</sup> T cells in skin-draining lymph nodes (SDLNs) from alopecic mice and naive mice. In the current study, we utilized mice with spontaneously developed AA (SpAA) as well as AA mice derived from adoptive transfer (AtAA; Methods). We found that the frequency of T<sub>VM</sub> cells was significantly higher among SDLNs from alopecic mice, compared to those from naive mice (Extended Data Fig. 1a). Notably, we observed that the T<sub>VM</sub> cell population among SDLNs from alopecic mice was subdivided into two distinct subpopulations based on differential CD44 expression levels: CD44<sup>hi</sup>CD49d<sup>lo</sup> CD8<sup>+</sup> T cells and conventional T<sub>VM</sub> cells (CD44<sup>hi</sup>CD49d<sup>lo</sup> CD8<sup>+</sup> T cells; Fig. 1a and Supplementary Fig. 1). This distinct cell population of CD44<sup>hi</sup>CD49d<sup>lo</sup> CD8<sup>+</sup> T cells was exclusively found in both SpAA and AtAA mice (Fig. 1b), and their CD44 expression level was much higher than that found in antigen-experienced CD44<sup>hi</sup>CD49d<sup>hi</sup> CD8<sup>+</sup> T cells from murine cytomegalovirus (MCMV)-infected or influenza A virus (IAV)-infected C3H/HeJ mice (Fig. 1a,b and Supplementary Fig. 2). In IAV-infected C3H/HeJ mice, most of the HA<sub>352-360</sub> dextramer<sup>+</sup> CD8<sup>+</sup> T cells were CD44<sup>hi</sup>CD49d<sup>hi</sup> cells, and were not CD49d<sup>lo</sup> cells (Supplementary Fig. 2a–c). More importantly, CD44<sup>hi</sup>CD49d<sup>lo</sup> CD8<sup>+</sup> T cells were exclusively observed in the skin of SpAA and AtAA mice, while conventional T<sub>VM</sub> cells were barely detected in these mice (Fig. 1c,d). Analysis of the proportions of CD44<sup>hi</sup>CD49d<sup>lo</sup> CD8<sup>+</sup> T cells in the SDLNs and skin revealed that the frequency did not significantly differ in SpAA versus AtAA mice (Fig. 1b,d). In alopecic mice, these CD44<sup>hi</sup>CD49d<sup>lo</sup> CD8<sup>+</sup> T cells were nearly absent in the spleen, liver, mesenteric lymph nodes and skin non-draining lymph nodes (Extended Data Fig. 1b).

Our results implied that this CD44<sup>hi</sup>CD49d<sup>lo</sup> CD8<sup>+</sup> T cell population may play an important role in AA pathogenesis, which was supported by our finding that the frequency of CD44<sup>hi</sup>CD49d<sup>lo</sup> CD8<sup>+</sup> T cells among SDLNs was associated with disease severity (Fig. 1e,f). To investigate the roles of CD44<sup>hi</sup>CD49d<sup>lo</sup> CD8<sup>+</sup> T cells as pathologic cells for AA, we isolated CD44<sup>hi</sup>CD49d<sup>lo</sup> CD8<sup>+</sup> T cells from SDLNs of AA mice, and adoptively transferred these cells into naive C3H/HeJ mice. Within 12 weeks after transfer, CD44<sup>hi</sup>CD49d<sup>lo</sup> CD8<sup>+</sup> T cells from alopecic mice induced AA in 91% of naive C3H/HeJ recipients (Fig. 1g,h), whereas conventional T<sub>VM</sub> cells from naive C3H/HeJ mice did not induce AA. Moreover, when C3H/HeJ recipients were adoptively transferred with T<sub>VM</sub> cells isolated from SDLNs of AA mice, a significant portion showed AA onset (Fig. 1h), although this AA induction occurred with a lower frequency and slower onset compared to that in mice adoptively transferred with CD44<sup>hi</sup>CD49d<sup>lo</sup> CD8<sup>+</sup> T cells. These findings suggest that CD44<sup>hi</sup>CD49d<sup>lo</sup> CD8<sup>+</sup> T cells might originate from conventional T<sub>VM</sub> cells.

To further characterize CD44<sup>hi</sup>CD49d<sup>lo</sup> CD8<sup>+</sup> T cells, we performed RNA-sequencing (RNA-seq) analysis to comprehensively investigate the gene expression profile differences between CD44<sup>hi</sup>CD49d<sup>lo</sup> CD8<sup>+</sup>

T cells from skin and SDLNs of AA mice, and T<sub>VM</sub> and T<sub>N</sub> cells from SDLNs of AA or age-matched naive mice. Gene clustering analysis revealed that CD44<sup>hi</sup>CD49d<sup>lo</sup> CD8<sup>+</sup> T cells from SDLNs and skin of SpAA and AtAA mice were clearly separated from other cell populations by principal component analysis (PCA; Fig. 1i). Additionally, the CD44<sup>hi</sup>CD49d<sup>lo</sup> CD8<sup>+</sup> T cells from skin of AA mice were distinct from those obtained from SDLNs of AA mice (Fig. 1i). PCA plots of RNA-seq data show similar characteristics between SpAA and AtAA (Fig. 1i). We identified a total of 199 genes (139 upregulated and 60 downregulated genes) that were distinctly expressed only in CD44<sup>hi</sup>CD49d<sup>lo</sup> CD8<sup>+</sup> T cells (Extended Data Fig. 1c and Supplementary Table 1). Direct comparison between the CD44<sup>hi</sup>CD49d<sup>lo</sup> CD8<sup>+</sup> T cells and T<sub>VM</sub> cells from SDLNs yielded identification of 1,034 differentially expressed genes, of which 163 were significantly upregulated and 871 significantly downregulated in CD44<sup>hi</sup>CD49d<sup>lo</sup> CD8<sup>+</sup> T cells (Supplementary Table 2). Notably, compared to the T<sub>VM</sub> cell population from SDLNs, the CD44<sup>hi</sup>CD49d<sup>lo</sup> CD8<sup>+</sup> T cell subpopulation from SDLNs exhibited marked enrichment of genes related to effector cytotoxic T lymphocytes (those encoding granzymes, *Ifng* and *Trif*), response to cytokines (*Cxcr6*, *Cx3cr1* and *Cd44*) and cell proliferation (*Il2ra* and *Cd40lg*; Fig. 1j,k). Additionally, compared to CD44<sup>hi</sup>CD49d<sup>lo</sup> CD8<sup>+</sup> T cells from SDLNs, those from skin of AA mice exhibited upregulation of genes related to cell motility and inflammatory response (Extended Data Fig. 1d,e and Supplementary Table 3). Gene set enrichment analysis (GSEA) also supports that genes related to T cell effector functions are highly enriched in CD44<sup>hi</sup>CD49d<sup>lo</sup> CD8<sup>+</sup> T cells from SDLNs of AA mice (Extended Data Fig. 2a,b).

### CD44<sup>hi</sup>CD49d<sup>lo</sup> CD8<sup>+</sup> T cells originate from T<sub>VM</sub> cells

Based on our results, we hypothesized that the pathologic CD44<sup>hi</sup>CD49d<sup>lo</sup> CD8<sup>+</sup> T cells originated from T<sub>VM</sub> cells. To show this, conventional T<sub>VM</sub> cells from SDLNs of AA mice were transduced with GFP-expressing retrovirus, and then the cells were adoptively transferred into C3H/HeJ mice (Fig. 2a,b). After transfer of GFP<sup>+</sup> T<sub>VM</sub> cells, we found GFP-expressing CD44<sup>hi</sup>CD49d<sup>lo</sup> CD8<sup>+</sup> T cell population in the skin of mice after AA development (Fig. 2c). To determine whether the TCR repertoires of CD44<sup>hi</sup>CD49d<sup>lo</sup> CD8<sup>+</sup> T cells overlapped with those of T<sub>VM</sub> cells, we sequenced the TCR CDR3 repertoires of these cell populations. Our data revealed that the TCR repertoire of CD44<sup>hi</sup>CD49d<sup>lo</sup> CD8<sup>+</sup> T cells largely overlapped with that of T<sub>VM</sub> cells from same donor (Fig. 2d). TCR diversity was decreased in CD44<sup>hi</sup>CD49d<sup>lo</sup> CD8<sup>+</sup> T cells compared to in T<sub>VM</sub> cells (Supplementary Fig. 3a,b). However, when CD44<sup>hi</sup>CD49d<sup>lo</sup> CD8<sup>+</sup> T cells from AA SDLNs were adoptively transferred into a naive C3H/HeJ mouse, the TCR diversity of CD44<sup>hi</sup>CD49d<sup>lo</sup> CD8<sup>+</sup> T cells did not substantially change between adoptively transferred CD44<sup>hi</sup>CD49d<sup>lo</sup> CD8<sup>+</sup> T cells and CD44<sup>hi</sup>CD49d<sup>lo</sup> CD8<sup>+</sup> T cells from SDLNs and skin of an AA developed mouse (Supplementary Fig. 3c,d).

To further investigate the transition of T<sub>VM</sub> cells to CD44<sup>hi</sup>CD49d<sup>lo</sup> CD8<sup>+</sup> T cells at a single-cell resolution, we performed cell fate trajectory and pseudotime analysis using Monocle 2 software for cell clusters<sup>16</sup>, including CD8<sup>+</sup> T<sub>N</sub> cells, T<sub>VM</sub> cells and Klrk1<sup>+</sup>CD8<sup>+</sup> T cells that predominantly express CD44 genes and genes related to T cell effector functions (representing CD44<sup>hi</sup>CD49d<sup>lo</sup> CD8<sup>+</sup> T cells; Extended Data Fig. 3a–d). Trajectory analysis revealed a continuum of cells, with a root corresponding predominantly to T<sub>N</sub> cells, and a terminal population corresponding to Klrk1<sup>+</sup>CD8<sup>+</sup> T cells by way of T<sub>VM</sub> cells (Fig. 2e). To investigate whether antigen-experienced conventional memory cells in the skin contributed to the induction of CD44<sup>hi</sup>CD49d<sup>lo</sup> CD8<sup>+</sup> T cells, naive C3H/HeJ mice were infected with vaccinia virus (VV) through the skin. At 12 weeks after adoptive transfer (AT), the overall disease-free ratio did not significantly differ between the VV-infected group and control groups (Extended Data Fig. 4a–d). Moreover, there was no significant difference in the frequencies of CD44<sup>hi</sup>CD49d<sup>lo</sup> CD8<sup>+</sup> T cells and their NKG2D geometric mean fluorescence intensity (gMFI) in the SDLNs of AA mice at 12 weeks between the VV-infected group and control group (Extended Data Fig. 4e–g). Collectively, our results show

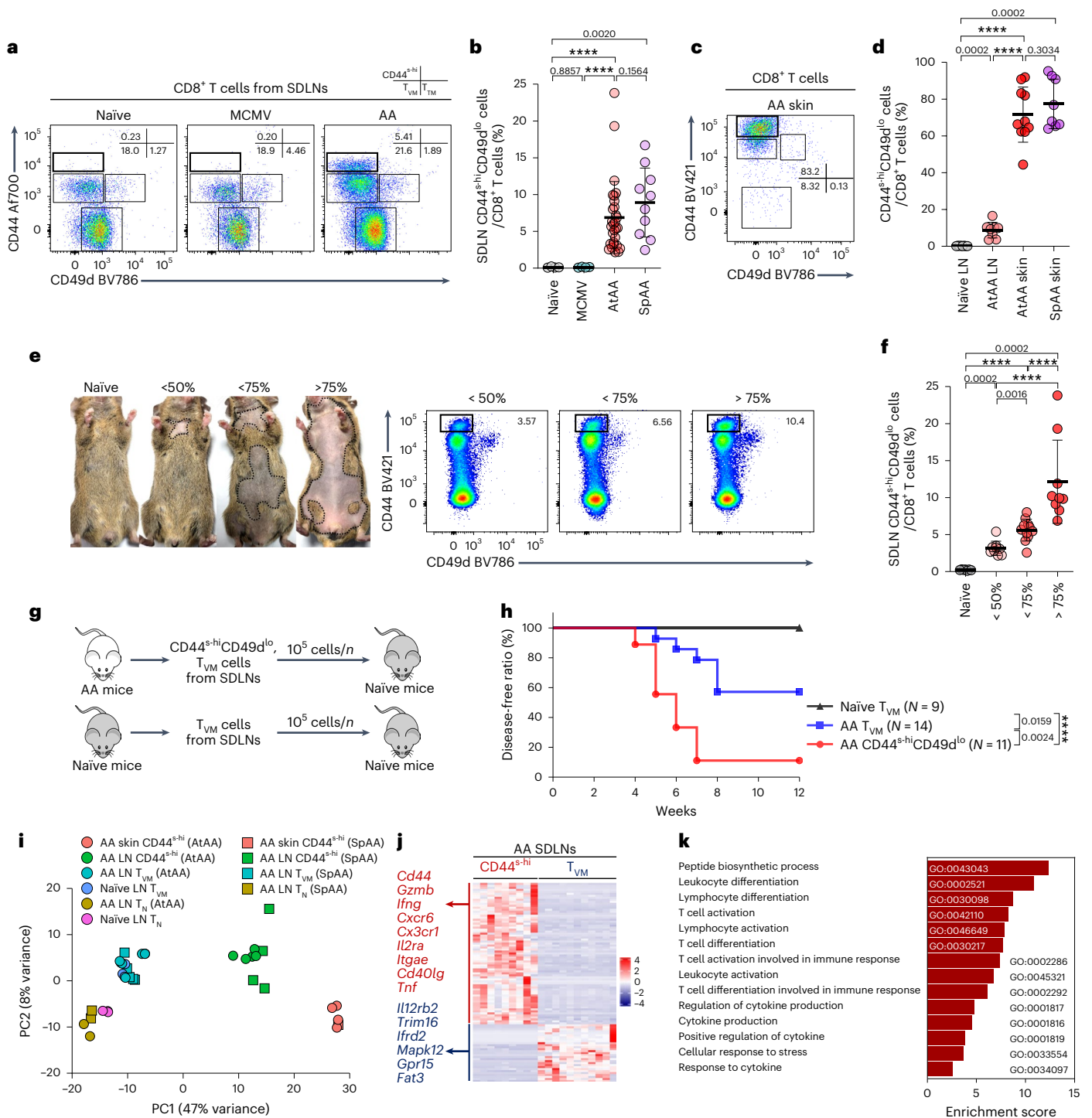


**Fig. 1** CD44<sup>hi</sup>CD49d<sup>lo</sup> CD8<sup>+</sup> T cell population causes alopecia areata. **a, b**, Frequency of CD44<sup>hi</sup>CD49d<sup>lo</sup> CD8<sup>+</sup> T cells in SDLNs from naive mice (*n* = 4), MCMV-infected mice (*n* = 4), AtAA mice (*n* = 29) and SpAA mice (*n* = 10; two independent experiments). **c, d**, Frequency of CD44<sup>hi</sup>CD49d<sup>lo</sup> CD8<sup>+</sup> T cells from both AtAA and SpAA skin, and SDLNs of AtAA mice and naive mice (*n* = 8, naive LN; *n* = 8, AtAA LN; *n* = 10, AtAA skin; *n* = 8, SpAA skin). Frequency values are shown in the crossed lines (**a** and **c**). **e, f**, Correlation between disease severity and the proportion of CD44<sup>hi</sup>CD49d<sup>lo</sup> cells among CD8<sup>+</sup> T cells from SDLNs (*n* = 7, naive; *n* = 9, <50%; *n* = 11, <75%; *n* = 9, >75%). **g**, Experimental scheme for testing whether CD44<sup>hi</sup>CD49d<sup>lo</sup> cells are required for AA pathogenesis. T<sub>VM</sub> cells from naive mice and AtAA mice, and CD44<sup>hi</sup>CD49d<sup>lo</sup> CD8<sup>+</sup> T cells from AtAA mice were adoptively transferred into 10-week-old naive female mice. **h**, AA development in

mice following the transfer of various cells (*n* = 9–14 per group). This experiment was independently repeated three times and the experimental findings were reliably reproduced. **i–k**, PCA (**i**), heat map of differentially expressed genes from SDLN CD44<sup>hi</sup>CD49d<sup>lo</sup> CD8<sup>+</sup> T cells compared to SDLN T<sub>VM</sub> cells (**j**) and enriched Gene Ontology (GO) biological process gene sets (adjusted *P* value < 0.05) (**k**) of differentially expressed genes in SDLN CD44<sup>hi</sup>CD49d<sup>lo</sup> CD8<sup>+</sup> T cells compared to SDLN T<sub>VM</sub> cells from MSigDB. The genes are ranked according to normalized enrichment score (NES). Data are the mean ± s.d. A Mann–Whitney test was performed for comparisons between two groups. A log-rank (Mantel–Cox) test was used for comparison of survival curves. All tests were two-sided, \*\*\*\**P* < 0.0001.

that CD44<sup>hi</sup>CD49d<sup>lo</sup> CD8<sup>+</sup> T cells originated from T<sub>VM</sub> cells, not from conventional memory CD8<sup>+</sup> T cells.

We next examined how CD44<sup>hi</sup>CD49d<sup>lo</sup> CD8<sup>+</sup> T cells could be induced from T<sub>VM</sub> cells. To date, no autoantigen that causes AA has been identified, and it is unclear whether autoantigen-specific T cells play a critical role in AA pathogenesis, including hair follicle destruction<sup>17–19</sup>. Therefore, we investigated whether there were common TCR sequences in CD44<sup>hi</sup>CD49d<sup>lo</sup> CD8<sup>+</sup> T cells among mice with SpAA. Comparing the TCR CDR3 $\beta$  nucleotide sequences and gene usage of CD44<sup>hi</sup>CD49d<sup>lo</sup> CD8<sup>+</sup> T cells between SpAA mice did not reveal overlapping TCR CDR3 $\beta$  sequences among alopecic mice (Supplementary Fig. 4a–c). CD44<sup>hi</sup>CD49d<sup>lo</sup> CD8<sup>+</sup> T cells did not show significant enrichment of genes involved in the TCR pathway (Fig. 2f). Moreover, the expression of Nur77, a specific marker of TCR signaling<sup>20,21</sup>, was not upregulated in CD44<sup>hi</sup>CD49d<sup>lo</sup> CD8<sup>+</sup> T cells from AA skin or SDLNs, compared to T<sub>N</sub> and T<sub>VM</sub> cells (Fig. 2g). In addition, the expressions of *Nr4a1*, *Nr4a2* and *Nr4a3* (which are upregulated by TCR signaling) were not upregulated in the SDLNs at 4 weeks after AT (before AA induction) and after AA onset (time point with high frequency of CD44<sup>hi</sup>CD49d<sup>lo</sup> CD8<sup>+</sup> T cells; Extended Data Fig. 5a,b). These results indicate that CD44<sup>hi</sup>CD49d<sup>lo</sup> CD8<sup>+</sup> T cells can be induced by TCR-independent mechanisms. Therefore, we hypothesized that cytokine stimulations might play an important role in the differentiation of T<sub>VM</sub> cells into CD44<sup>hi</sup>CD49d<sup>lo</sup> CD8<sup>+</sup> T cells. Notably, among T<sub>VM</sub> cells from both AA mice and naive mice, in vitro treatment with IL-12, IL-15 or IL-18 induced generation of CD44<sup>hi</sup>CD49d<sup>lo</sup> CD8<sup>+</sup> T cells (Fig. 2h–j). More importantly, combined stimulation with IL-12, IL-15 and IL-18 led to the most efficient generation of CD44<sup>hi</sup>CD49d<sup>lo</sup> CD8<sup>+</sup> T cells (Fig. 2h–j), whereas CD44<sup>hi</sup>CD49d<sup>lo</sup> CD8<sup>+</sup> T cells were not induced from T<sub>N</sub> cells after in vitro treatment with cytokines (Extended Data Fig. 6a).

Next, to further confirm the results, T<sub>VM</sub> cells isolated from naive C3H/HeJ mice were stimulated in vitro with IL-12, IL-15 and IL-18 for 7 days, and then these cells were adoptively transferred into naive C3H/HeJ mice (Fig. 3a). When recipients were adoptively transferred with cultured T<sub>VM</sub> cells from naive C3H/HeJ mouse, 6 of 11 mice developed AA with a higher frequency of CD44<sup>hi</sup>CD49d<sup>lo</sup> CD8<sup>+</sup> T cells in their skin and SDLNs, while no mice transferred with unstimulated T<sub>VM</sub> cells developed AA ( $P < 0.01$ ; Fig. 3b and Extended Data Fig. 6b). When C57BL/6 or BALB/c recipients were adoptively transferred with cytokine-stimulated T<sub>VM</sub> cells from each mouse strain, none of the adoptively transferred mice developed AA until 12 weeks after AT, although in vitro treatment with IL-12, IL-15 or IL-18 induced the in vitro generation of CD44<sup>hi</sup>CD49d<sup>lo</sup> CD8<sup>+</sup> T cells from T<sub>VM</sub> cells (Supplementary Fig. 5a–c).

We used confocal microscopy analyses and ELISA assays to examine the expression levels of IL-12, IL-15 and IL-18 in skin, and we found significantly increased expression of these cytokines in SpAA and AtAA mice, compared to naive mice (Fig. 3c,d and Supplementary Fig. 6a). We also examined human skin specimens from patients with AA and found notably increased IL-12, IL-15 and IL-18 levels in the skin of individuals with AA compared to skin from healthy volunteers (Extended Data Fig. 7a). To translate the findings from preclinical models into human disease, we analyzed previously reported AA single-cell RNA-seq data<sup>22</sup>.

Of the identified clusters, the *KLRC3*<sup>+</sup> CD8<sup>+</sup> T cell population was an AA-predominant clusters (Extended Data Fig. 7b). This group exhibited high expression levels of *KLRC1*, *KIR2DL1*, *KIR2DL4*, *KIR3DL1*, *KIR3DL2* and *KLRK1*, which have been suggested as genes encoding human T<sub>VM</sub> cell markers (Extended Data Fig. 7c)<sup>7,23</sup>. In AA human skin, CD8<sup>+</sup> T cells with T<sub>VM</sub> features (KIR<sup>+</sup>NKG2A<sup>+</sup>CD8<sup>+</sup> T cells) were predominantly infiltrated in the hair follicles (Extended Data Fig. 7d). In addition, we observed that the frequency of CD8<sup>+</sup> T cells with T<sub>VM</sub> features in peripheral blood was significantly higher in individuals with AA than healthy volunteers (Extended Data Fig. 7e).

To further investigate the roles of IL-12, IL-15 and IL-18 in the development of CD44<sup>hi</sup>CD49d<sup>lo</sup> CD8<sup>+</sup> T cells in vivo, we injected mice with blocking antibodies to IL-12, IL-15R $\beta$  and IL-18 starting at the time of AT of T<sub>VM</sub> cells from AA mice into naive C3H/HeJ mice (Fig. 3e). Combined administration of anti-IL-12, anti-IL-15R $\beta$  and anti-IL-18 antibodies completely prevented AA development in all recipient mice ( $P < 0.05$ ), whereas AA developed in 10 of 20 mice that were transferred with T<sub>VM</sub> cells without blocking antibody administration (Fig. 3e). Administration of anti-IL-12/anti-IL-18 or anti-IL-15R $\beta$  showed partial effects in terms of the disease-free ratio and the time of disease onset (Fig. 3e).

Collectively, these results demonstrate that CD44<sup>hi</sup>CD49d<sup>lo</sup> CD8<sup>+</sup> T cells are induced from T<sub>VM</sub> cells via stimulation with IL-12, IL-15 and IL-18, and can cause a chronic inflammatory disease, AA.

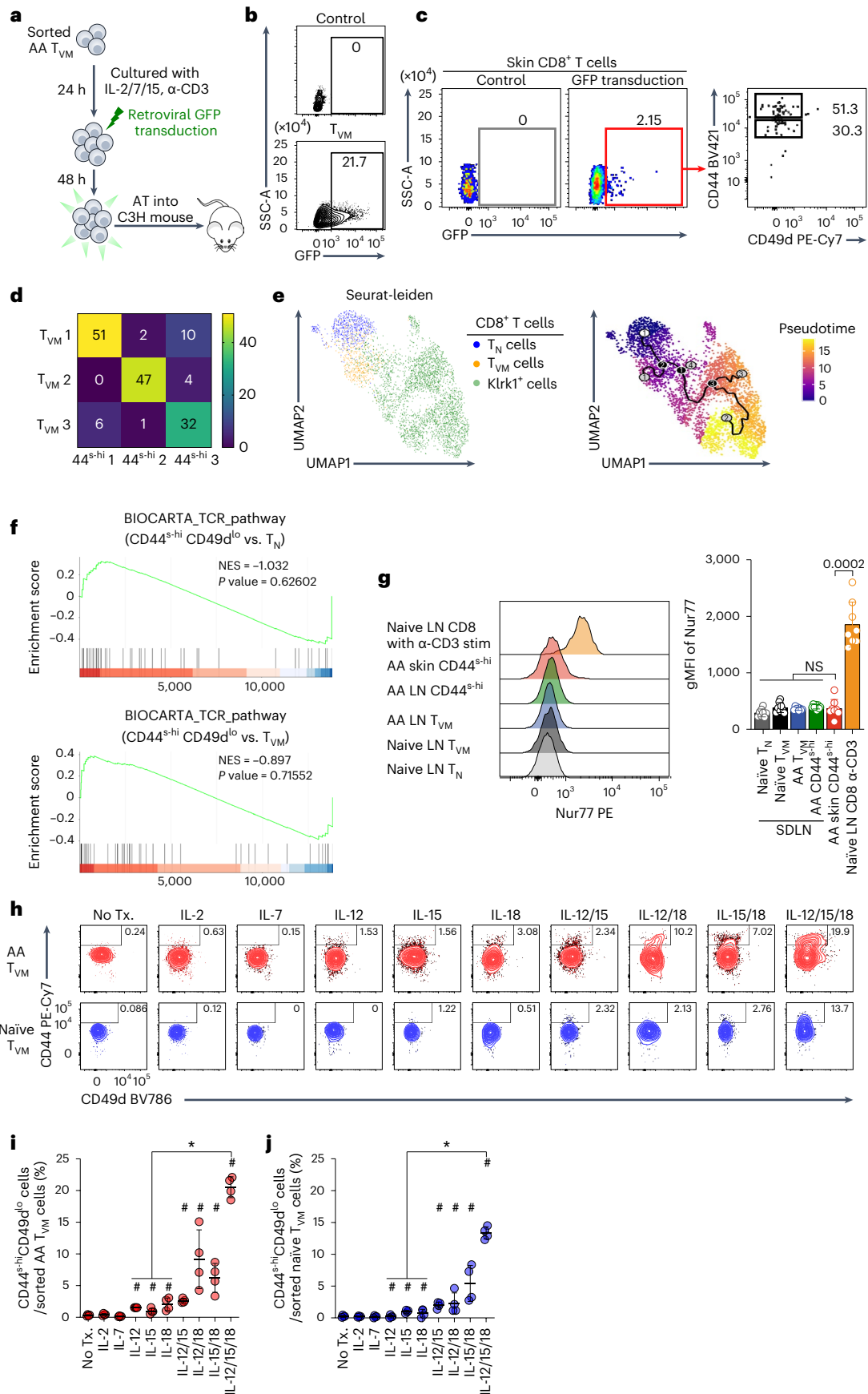
### CD44<sup>hi</sup>CD49d<sup>lo</sup> CD8<sup>+</sup> T cells have strong effector function

Next, we investigated the mechanisms of how CD44<sup>hi</sup>CD49d<sup>lo</sup> CD8<sup>+</sup> T cells gain cytotoxic activity and cause the immunopathogenesis of a chronic inflammatory disease, AA. Ex vivo analyses of CD44<sup>hi</sup>CD49d<sup>lo</sup>, T<sub>VM</sub> and T<sub>N</sub> CD8<sup>+</sup> T cells revealed that the skin CD44<sup>hi</sup>CD49d<sup>lo</sup> CD8<sup>+</sup> T cell subpopulation produced the highest amounts of granzyme B and perforin, compared to other groups (Fig. 4a,b). Similarly, the skin CD44<sup>hi</sup>CD49d<sup>lo</sup> CD8<sup>+</sup> T cells produced the highest amounts of interferon- $\gamma$  (IFN $\gamma$ ) and tumor necrosis factor (TNF; Fig. 4a,c).

It has been suggested that AA pathogenesis is mediated through NKG2D-dependent cytotoxicity exerted by CD8<sup>+</sup> T cells against dermal sheath target cells<sup>15</sup>, although it is unknown which CD8<sup>+</sup> T cell subset induces innate-like cytotoxicity. Upon showing that CD44<sup>hi</sup>CD49d<sup>lo</sup> CD8<sup>+</sup> T cells are major pathologic cells in AA, we next evaluated their NKG2D expression. We found significantly higher NKG2D expression in CD44<sup>hi</sup>CD49d<sup>lo</sup> CD8<sup>+</sup> T cells from skin and SDLNs, compared to T<sub>N</sub> and T<sub>VM</sub> CD8<sup>+</sup> T cells at both protein (Fig. 4d) and mRNA (Fig. 4e) levels. The expression of NKG2D ligand Rae-1 was predominantly observed in the skin of AA mice (Supplementary Fig. 7a). We observed that CD8<sup>+</sup> T cells with T<sub>VM</sub> features in individuals with AA exhibited upregulated NKG2D expression (Extended Data Fig. 7f). Additionally, CD44<sup>hi</sup>CD49d<sup>lo</sup> CD8<sup>+</sup> T cells from AA mice included significantly larger percentages of Ki-67<sup>+</sup> cells, a marker of proliferating cells (Fig. 4f). Moreover, when we investigated expression levels of the skin tissue-resident memory T (T<sub>RM</sub>) cell markers CD103 and CD49a, we found that almost all CD44<sup>hi</sup>CD49d<sup>lo</sup> CD8<sup>+</sup> T cells in skin were CD103<sup>+</sup>CD49a<sup>+/+</sup> (Fig. 4g). This was confirmed by GSEA showing that genes related to T<sub>RM</sub> cell features were highly enriched in CD44<sup>hi</sup>CD49d<sup>lo</sup> CD8<sup>+</sup> T cells from skin compared to in CD44<sup>hi</sup>CD49d<sup>lo</sup> and T<sub>VM</sub> CD8<sup>+</sup> T cells from SDLNs of AA mice (Extended

**Fig. 2 | CD44<sup>hi</sup>CD49d<sup>lo</sup> CD8<sup>+</sup> T cells originate from T<sub>VM</sub> cells.** **a**, Experimental scheme for testing whether AA T<sub>VM</sub> cells differentiate into CD44<sup>hi</sup>CD49d<sup>lo</sup> CD8<sup>+</sup> T cells. T<sub>VM</sub> cells were retrovirally transduced with GFP, and then adoptively transferred (AT) into C3H/HeJ mice. **b**, Transduction efficiency of the T<sub>VM</sub> cells. **c**, Representative flow cytometry plot of GFP<sup>+</sup> CD8<sup>+</sup> T cells in the skin of AA mice. **d**, Heat map showing the number of clonotypes shared between the CD44<sup>hi</sup>CD49d<sup>lo</sup> and T<sub>VM</sub> cell populations of SpAA. **e**, Pseudotime analysis of single CD8<sup>+</sup> cells using Monocle 2. **f**, GSEA was performed to measure the enrichment of specific gene sets from BIOCARTA\_TCR\_PATHWAY among CD44<sup>hi</sup>CD49d<sup>lo</sup> CD8<sup>+</sup> T cells compared to naive CD8<sup>+</sup> T cells or T<sub>VM</sub> cells. **g**, Nur77 MFI was compared between each cell population ( $n = 8$  per group). For a positive

control of Nur77 expression, SDLN CD8<sup>+</sup> T cells were stimulated with anti-CD3 for 5 h. **h–j**, In vitro stimulation of T<sub>VM</sub> cells with various cytokines. As shown in representative flow cytometry plots (**h**), AA T<sub>VM</sub> cells (**i**) and naive T<sub>VM</sub> cells (**j**) were incubated with IL-2, IL-7, IL-12, IL-15 or IL-18 for 3 days and analyzed by flow cytometry. Cytokines were used at fixed doses: 50 ng ml<sup>-1</sup> IL-2, 50 ng ml<sup>-1</sup> IL-7, 50 ng ml<sup>-1</sup> IL-12, 50 ng ml<sup>-1</sup> IL-15 and 50 ng ml<sup>-1</sup> IL-18 ( $n = 4$  per group). Except for **d**, data were acquired from AtAA mice. Data are the mean  $\pm$  s.d. A Mann–Whitney test was performed for comparisons between two groups. All tests were two sided. NS, not significant, \* $P < 0.05$ , #Assessed using  $P$  values comparing various cytokine stimulations to no treatment ( $P < 0.05$ ).



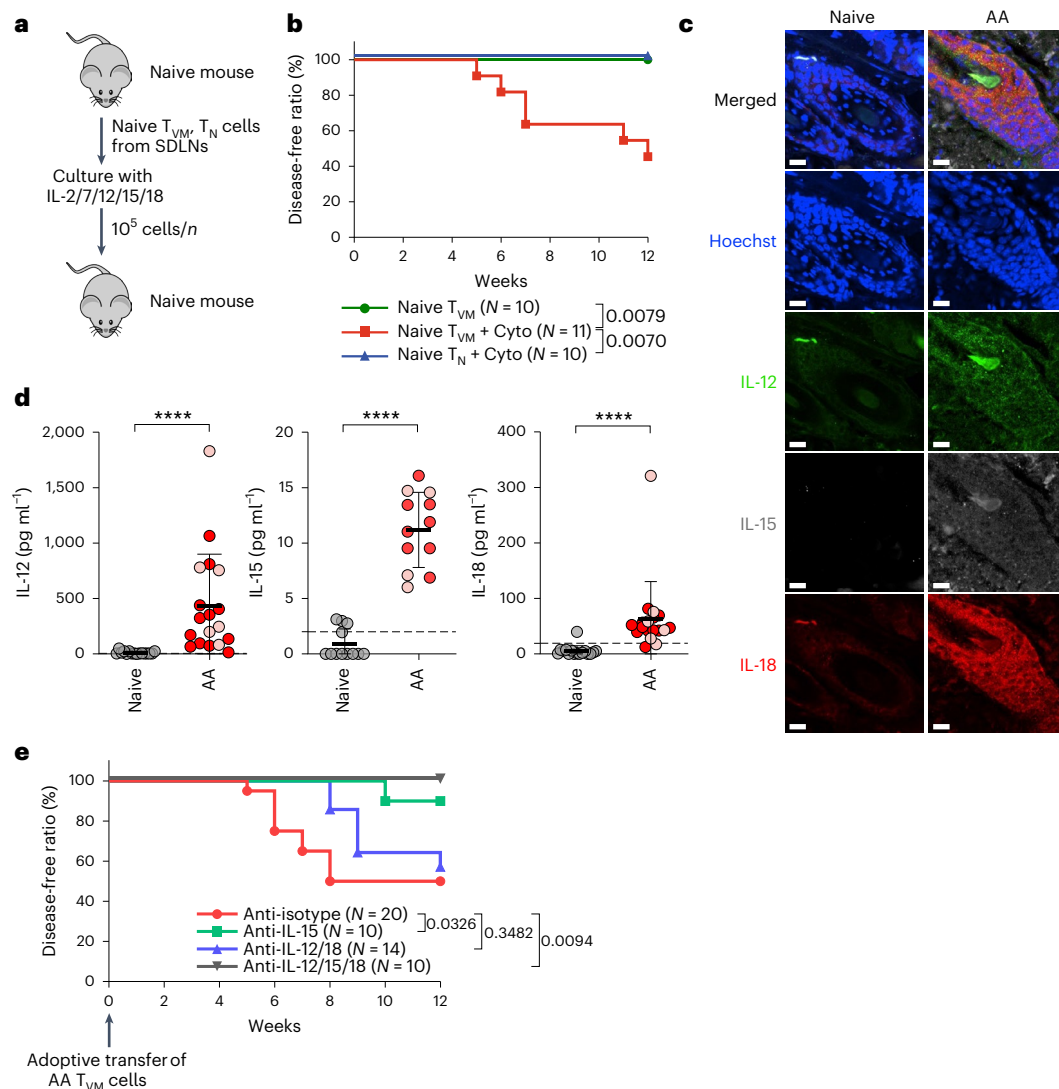


**Fig. 3 | CD44<sup>hi</sup>CD49d<sup>lo</sup>CD8<sup>+</sup> T cells are derived from T<sub>VM</sub> cells by cytokine stimulation.** **a**, Experimental scheme for investigating the roles of cytokines in the induction of CD44<sup>hi</sup>CD49d<sup>lo</sup>CD8<sup>+</sup> T cells from naive T<sub>VM</sub> cells. Naive T<sub>VM</sub> cells and naive T<sub>N</sub> cells were stimulated with IL-12/IL-15/IL-18 for 7 days, and then transferred into naive C3H/HeJ mice. **b**, AA development in mice with transferred naive T<sub>VM</sub> cells and naive T<sub>N</sub> cells with cytokine stimulation ( $n = 10$ –11 per group). This experiment was independently repeated three times and the experimental findings were reliably reproduced. **c**, Immunofluorescence staining of the skin of naive and SpAA mice revealed upregulation of IL-12, IL-15 and IL-18 in the hair follicles. Scale bars, 15  $\mu$ m. This experiment was independently repeated three times and the experimental findings were reliably

reproduced. **d**, IL-15–IL-15R complex ( $n = 16$  per group), IL-12 ( $n = 16$ , naive;  $n = 18$ , AA) and IL-18 ( $n = 16$ , naive;  $n = 18$ , AA) were measured in the skin of AA and naive mice by ELISA. Red and pink circles indicate the data from AtAA and SpAA mice, respectively. **e**, In naive mice with transferred AtAA T<sub>VM</sub> cells, AA development was monitored during systemic administration with antibodies to IL-15, IL-12/IL-18 and IL-12/IL-15/IL-18, compared to that of isotype-treated mice ( $n = 10$ –20 per group). This experiment was independently repeated three times and the experimental findings were reliably reproduced. Data are the mean  $\pm$  s.d. A Mann–Whitney test was performed for comparisons between two groups. A log-rank (Mantel–Cox) test was used for comparison of survival curves. All tests were two sided. \*\*\*\* $P < 0.0001$ .

Data Fig. 8a,b)<sup>24</sup>. Together, our results indicate that CD44<sup>hi</sup>CD49d<sup>lo</sup>CD8<sup>+</sup> T cells in AA skin are a distinct cell population having strong effector functions and proliferative capacity with T<sub>RM</sub> cell features.

Our results indicate that CD44<sup>hi</sup>CD49d<sup>lo</sup>CD8<sup>+</sup> T cells can be induced from T<sub>VM</sub> cells via stimulation with cytokines. Therefore, we investigated whether cytokine stimulation could enhance the effector functions and proliferative capacity of CD44<sup>hi</sup>CD49d<sup>lo</sup>CD8<sup>+</sup> T cells. IL-2, IL-7 and IL-15 each significantly increased the percentage of granzyme B<sup>+</sup> and perforin<sup>+</sup>CD44<sup>hi</sup>CD49d<sup>lo</sup>CD8<sup>+</sup> T cells (Fig. 4h and Extended Data Fig. 9a). Analysis of cytokine production revealed that IL-12 and IL-12/IL-18 significantly increased the production of IFN $\gamma$  and TNF by CD44<sup>hi</sup>CD49d<sup>lo</sup>CD8<sup>+</sup> T cells (Fig. 4i and Extended Data Fig. 9b). Compared to other cell populations, CD44<sup>hi</sup>CD49d<sup>lo</sup>CD8<sup>+</sup> T cells

produced the largest amounts of IFN $\gamma$ , TNF and granzyme B following cytokine stimulation (Extended Data Fig. 9c). The proliferation of CD44<sup>hi</sup>CD49d<sup>lo</sup>CD8<sup>+</sup> T cells was significantly enhanced by IL-2, IL-7 and IL-15, but not by IL-12 and IL-18 (Fig. 4j and Extended Data Fig. 9d,e). Moreover, IL-15 stimulation further increased the NKG2D expression on CD44<sup>hi</sup>CD49d<sup>lo</sup>CD8<sup>+</sup> T cells (Fig. 4k and Extended Data Fig. 9f,g).

#### NKG2D-dependent cytotoxicity of CD44<sup>hi</sup>CD49d<sup>lo</sup>CD8<sup>+</sup> T cells

Finally, we investigated whether T<sub>VM</sub>-originated CD44<sup>hi</sup>CD49d<sup>lo</sup>CD8<sup>+</sup> T cells induced innate-like cytotoxic activity in an NKG2D-dependent manner. We found that CD44<sup>hi</sup>CD49d<sup>lo</sup>CD8<sup>+</sup> T cells readily exerted cytotoxic activity against YAC-1 cells, and that IL-15 enhanced the killing

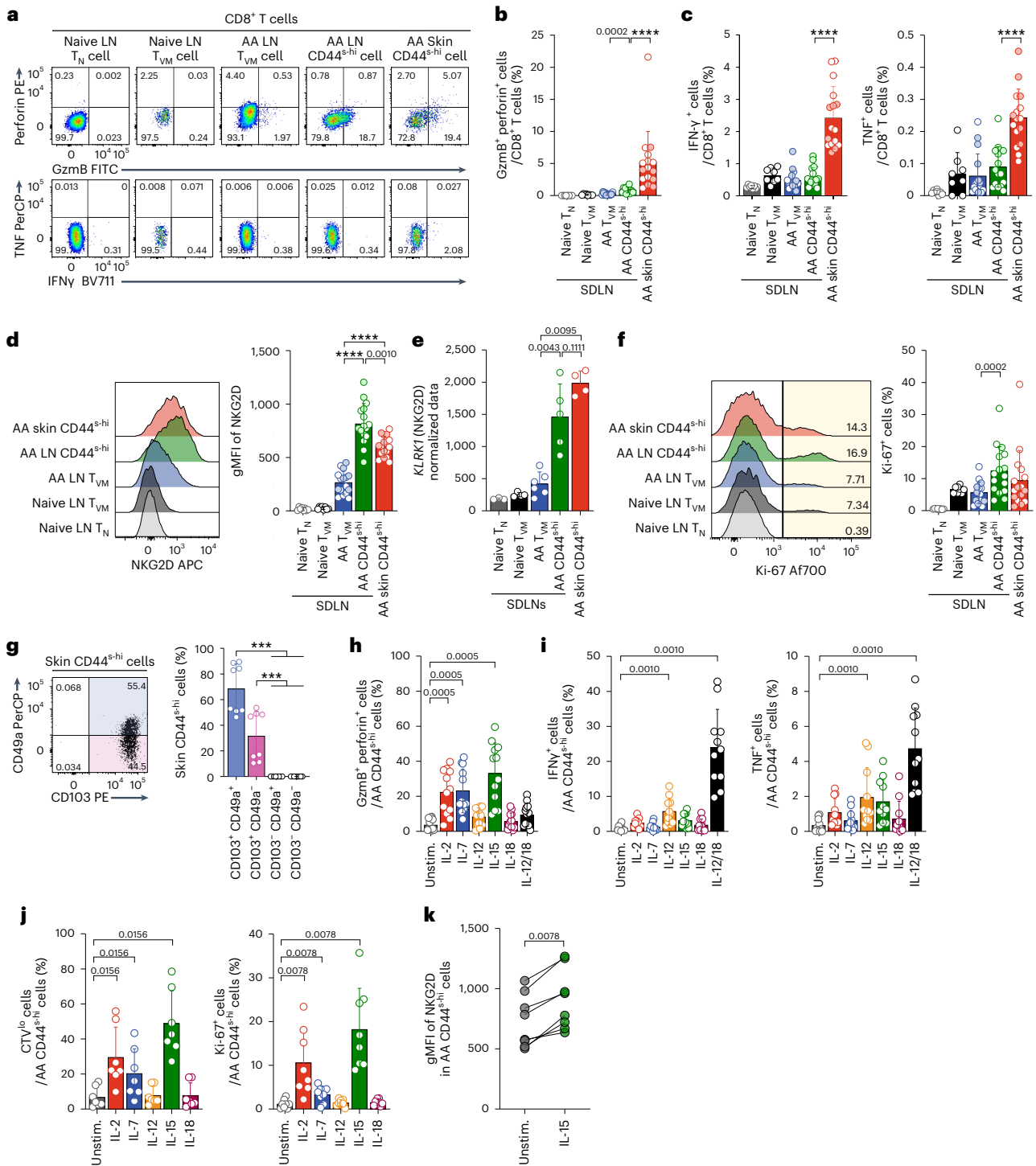


**Fig. 4 | CD44<sup>hi</sup>CD49d<sup>lo</sup> CD8<sup>+</sup> T cells have strong effector functions with T<sub>RM</sub> cell features.** **a–c**, Harvested cells were incubated with GolgiPlug and GolgiStop for 5 h without stimulation, and then stained for intracellular markers as indicated. White and lightly colored circles indicate the data from AtAA and SpAA mice, respectively. Representative flow cytometry plot of each cell population in ex vivo sample are shown (**a**). Granzyme B (GzmB)<sup>+</sup> and perforin<sup>+</sup> (*n* = 8, naive; *n* = 16, AA) (**b**), and IFN $\gamma$ <sup>+</sup> and TNF<sup>+</sup> cells (*n* = 8, naive; *n* = 16, AA) (**c**) were assessed in each cell population. **d**, gMFI of the NKG2D level in each cell population (*n* = 8, Naive; *n* = 16, AA). **e**, KLRK1 gene-normalized data from RNA-seq data (*n* = 3, naive T<sub>N</sub>; *n* = 4, naive T<sub>VM</sub>; *n* = 6, AA T<sub>VM</sub>; *n* = 5, AA CD44<sup>hi</sup>; *n* = 4, AA skin CD44<sup>hi</sup>). **f**, The percentage of Ki-67<sup>+</sup> cells in each cell population (*n* = 8, naive; *n* = 16, AA). **g**, The percentage of CD103<sup>+</sup>CD49a<sup>-</sup> cells among skin CD44<sup>hi</sup>CD49d<sup>lo</sup> CD8<sup>+</sup> T cells (*n* = 8 per group). **h, i**, Following stimulation with

various cytokines, CD44<sup>hi</sup>CD49d<sup>lo</sup> CD8<sup>+</sup> T cells from SDLNs were incubated for 48 h and intracellular cytokine staining performed to examine the percentage of GzmB<sup>+</sup> and perforin<sup>+</sup> cells (*n* = 12) (**h**) or the percentage of IFN $\gamma$ <sup>+</sup> and TNF<sup>+</sup> cells (*n* = 11) (**i**). Cytokines were IL-2 (50 ng ml<sup>-1</sup>), IL-7 (50 ng ml<sup>-1</sup>), IL-12 (50 ng ml<sup>-1</sup>), IL-15 (50 ng ml<sup>-1</sup>) and IL-18 (50 ng ml<sup>-1</sup>). **j**, Following cytokine stimulation, CD44<sup>hi</sup>CD49d<sup>lo</sup> CD8<sup>+</sup> T cells were incubated for 96 h and analyzed for the percentage of CellTrace Violet<sup>lo</sup> (CTV<sup>lo</sup>) cells (*n* = 7) or incubated for 48 h and analyzed for the percentage of Ki-67<sup>+</sup> cells (*n* = 8). **k**, Comparison of the gMFI of NKG2D among CD44<sup>hi</sup>CD49d<sup>lo</sup> CD8<sup>+</sup> T cells without stimulation or in the presence of IL-15 (*n* = 8). Data are the mean  $\pm$  s.d. A Mann–Whitney test was performed for comparisons between two groups. A Wilcoxon test was performed for pairwise comparison between two groups (**h–k**). All tests were two sided. \*\*\**P* < 0.001, \*\*\*\**P* < 0.0001.

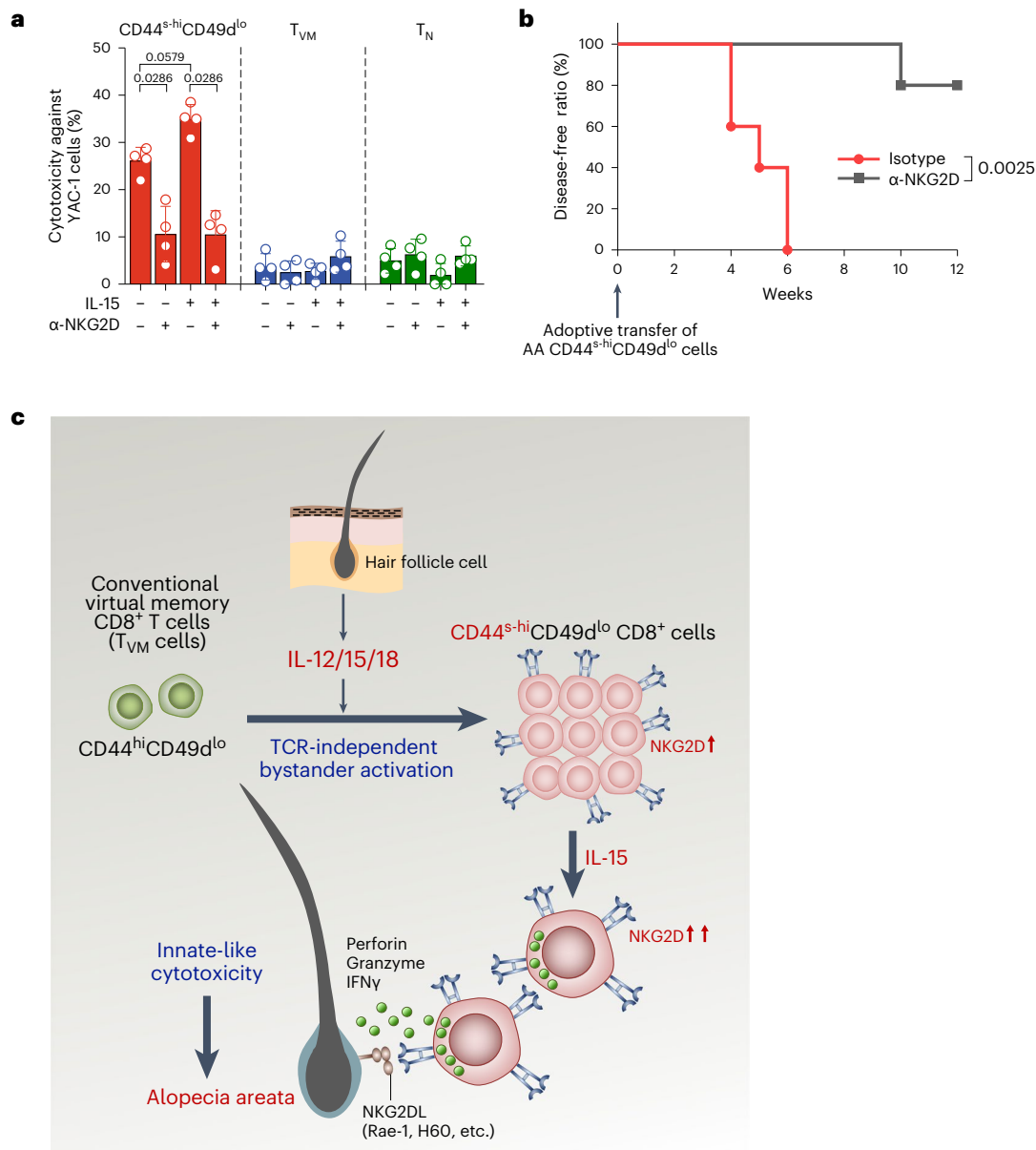


**Fig. 5 | Cytolytic activity of CD44<sup>S-HI</sup>CD49d<sup>LO</sup> CD8<sup>+</sup> T cells is abrogated by NKG2D blockade.** **a**, Cytolytic activity of CD44<sup>S-HI</sup>CD49d<sup>LO</sup> CD8<sup>+</sup> T cells, T<sub>VM</sub> cells and T<sub>N</sub> cells isolated from AA mice in the presence of IL-15 and/or anti-NKG2D (10  $\mu$ g ml<sup>-1</sup>) with 20 min of pre-incubation against YAC-1 cells at an effector-to-target ratio of 20:1 ( $n = 4$  per group). **b**, AA development in mice with transferred AA CD44<sup>S-HI</sup>CD49d<sup>LO</sup> CD8<sup>+</sup> T cells and systemic treatment with antibodies to

NKG2D from the time of AT compared to isotype-treated mice ( $n = 5$  per group). **c**, Model of induction and roles of CD44<sup>S-HI</sup>CD49d<sup>LO</sup> CD8<sup>+</sup> T cells in AA. Data are the mean  $\pm$  s.d. A Mann-Whitney test was performed for comparisons between two groups. A log-rank (Mantel-Cox) test was used for comparison of survival curves. All tests were two sided.

of YAC-1 cells by CD44<sup>S-HI</sup>CD49d<sup>LO</sup> CD8<sup>+</sup> T cells (Fig. 5a). It is known that the epithelial layers of hair follicles overexpress NKG2DLs and IL-15 (ref. 15). Importantly, cytotoxicity against YAC-1 cells was significantly blocked by anti-NKG2D treatment of CD44<sup>S-HI</sup>CD49d<sup>LO</sup> CD8<sup>+</sup> T cells, and not of T<sub>N</sub> and T<sub>VM</sub> cells (Fig. 5a). To investigate how the NKG2D-dependent cytotoxicity of CD44<sup>S-HI</sup>CD49d<sup>LO</sup> CD8<sup>+</sup> T cells contributed to AA pathogenesis in vivo, we administered blocking anti-NKG2D to C3H/HeJ mice that were adoptively transferred with CD44<sup>S-HI</sup>CD49d<sup>LO</sup> CD8<sup>+</sup> T cells. Within 6 weeks after AT of CD44<sup>S-HI</sup>CD49d<sup>LO</sup> CD8<sup>+</sup> T cells, AA developed in only one of the five anti-NKG2D-treated mice, and in all mice without anti-NKG2D treatment ( $P < 0.01$ ; Fig. 5b). We also observed that compared to isotype control mice, the anti-NKG2D-treated mice exhibited a significantly lower frequency of CD44<sup>S-HI</sup>CD49d<sup>LO</sup> CD8<sup>+</sup> T cells in SDLNs (Supplementary Fig. 8a).

Overall, our results suggest that CD44<sup>S-HI</sup>CD49d<sup>LO</sup> CD8<sup>+</sup> T cells that were originated from T<sub>VM</sub> cells induced AA pathogenesis through NKG2D-mediated innate-like cytotoxicity. These findings imply that anti-NKG2D treatment would be a promising therapeutic strategy for curing CD44<sup>S-HI</sup>CD49d<sup>LO</sup> CD8<sup>+</sup> T cell-mediated chronic inflammatory diseases, including AA.

## Discussion

Our present results identified a pathogenic cytotoxic CD8<sup>+</sup> subset that originates from T<sub>VM</sub> cells by cytokine stimulations and can cause chronic inflammatory diseases. To our knowledge, this is the first study to answer the question of whether T<sub>VM</sub> cells contribute to the immunopathogenesis of chronic inflammatory diseases. Our data reveal that T<sub>VM</sub>-originated CD44<sup>S-HI</sup>CD49d<sup>LO</sup> CD8<sup>+</sup> T cells could be



induced by combined stimulation with cytokines such as IL-12, IL-15 and IL-18 (Fig. 5c). The cells had activated phenotypes and enhanced proliferation capacity compared to conventional  $T_{VM}$  cells and  $T_N$  cells. Moreover, in humans with AA, we observed that IL-12, IL-15 and IL-18 expressions were upregulated exclusively in their alopecic skin. The frequencies of peripheral  $CD8^+$  T cells with  $T_{VM}$  features (KIR<sup>+</sup>NKG2A<sup>+</sup>) and of NKG2D-upregulated KIR<sup>+</sup>NKG2A<sup>+</sup>  $CD8^+$  T cells in skin were much higher in individuals with AA compared to healthy individuals. Further clinical studies are warranted to investigate the detailed immunological characteristics and the exact roles of the  $T_{VM}$ -originated pathologic cell population in individuals with AA that corresponds to the  $CD44^{s-hi}CD49d^{lo}CD8^+$  T cells that we discovered in mice.

One unresolved question in AA is whether autoantigens and autoreactive T cells contribute to disease pathogenesis. In our study, we found that pathologic  $CD44^{s-hi}CD49d^{lo}CD8^+$  T cells were generated from conventional  $T_{VM}$  cells by cytokine stimulations and that the activation and NKG2D-mediated cytolytic activity of  $CD44^{s-hi}CD49d^{lo}CD8^+$  T cells were further enhanced by cytokine stimulations. Autoantigen epitopes in AA have not been identified in mice with AA development, or in humans with AA. Although the experimental evidence shown in the current study suggests that cytokine stimulation, not antigen-driven expansion, is the main mechanism for the generation of  $CD44^{s-hi}CD49d^{lo}CD8^+$  T cells from  $T_{VM}$  cells, the need for antigen-driven expansion of  $T_{VM}$  cells during the early stage of AA development cannot be completely ruled out. For example, given that TCR diversity was decreased in  $CD44^{s-hi}CD49d^{lo}CD8^+$  T cells compared to in  $T_{VM}$  cells, it could be possible that a small number of  $T_{VM}$  cells with a broad repertoire enter the skin and undergo clonal expansion and reside in the skin by antigen-dependent mechanisms. In a future study, the detailed mechanisms underlying this phenomenon need to be further investigated. Moreover, our results suggest that cytotoxic activity of  $T_{VM}$ -originated  $CD44^{s-hi}CD49d^{lo}CD8^+$  T cells is mediated by IL-15-induced NKG2D. It appears that upregulated expression of NKG2DLs in hair follicles of humans with AA and their interaction with NKG2D on  $CD44^{s-hi}CD49d^{lo}CD8^+$  T cells play an essential role<sup>25</sup>. Recent reports describe a strong correlation between AA and the occurrence of various chronic immune-mediated inflammatory diseases such as autoimmune thyroiditis, vitiligo and myocardial infarction<sup>26–28</sup>. Therefore, considering that  $CD44^{s-hi}CD49d^{lo}CD8^+$  T cells can induce NKG2D-mediated TCR-independent innate-like cytotoxicity, these cells may contribute to the pathogenesis of these other immune-mediated inflammatory diseases.

$T_{VM}$  cells express CXCR3 at high levels compared to  $T_N$  cells, and their ligands CXCL9 and CXCL10 are upregulated in the skin of AA<sup>3,29,30</sup>. Therefore, it is possible that  $T_{VM}$  cells migrate to the skin where they are stimulated by cytokines to become tissue-resident pathologic  $CD44^{s-hi}CD49d^{lo}CD8^+$  T cells. In this study, it was confirmed that  $T_{VM}$  cells are the source of  $CD44^{s-hi}CD49d^{lo}CD8^+$  T cells in the skin, but no comparison was made with other cell populations such as antigen-experienced memory T cells or naive T cells in terms of their ability to migrate to or retain in the skin. Therefore, it will be of interest to investigate whether  $T_{VM}$  cells are more efficient at trafficking to the tissues or retention in the tissues compared to memory T cells. Another interesting finding is that when  $T_{VM}$  cells were adoptively transferred into naive C3H/HeJ mice, AA was induced by  $T_{VM}$  cells isolated from AA mice (AA  $T_{VM}$  cells) but not by  $T_{VM}$  cells isolated from naive mice (naive  $T_{VM}$  cells), suggesting the transition from  $T_{VM}$  cells to  $CD44^{s-hi}CD49d^{lo}CD8^+$  T cells. A key difference between AA  $T_{VM}$  cells and naive  $T_{VM}$  cells is that the former might experience an inflammatory milieu in the skin, which may activate  $T_{VM}$  cells. Additionally, we found that genes associated with negative regulation of cellular process and chromatin remodeling were significantly highly enriched in AA  $T_{VM}$  cells compared to naive  $T_{VM}$  cells. This leads us to propose that during the transition of conventional  $T_{VM}$  cells into  $CD44^{s-hi}CD49d^{lo}CD8^+$  T cells, inflammatory

cytokines may drive distinct epigenetic changes. Future research is needed to further study the epigenetic changes between AA  $T_{VM}$  cells, naive  $T_{VM}$  cells and  $CD44^{s-hi}CD49d^{lo}CD8^+$  T cells, which might provide valuable clues regarding the molecular mechanisms through which  $CD44^{s-hi}CD49d^{lo}CD8^+$  T cells are induced from  $T_{VM}$  cells.

In conclusion, here we demonstrated the existence of a pathologic  $CD8^+$   $T_{VM}$  cell population, which can be generated by cytokine stimulation and cause chronic inflammatory diseases. We further found that the cytotoxic activity of  $T_{VM}$ -originated  $CD44^{s-hi}CD49d^{lo}CD8^+$  T cells can be abrogated by NKG2D blockade, which will help guide the development of new therapeutic strategies against these kinds of diseases.

## Online content

Any methods, additional references, Nature Portfolio reporting summaries, source data, extended data, supplementary information, acknowledgements, peer review information; details of author contributions and competing interests; and statements of data and code availability are available at <https://doi.org/10.1038/s41590-023-01547-5>.

## References

- Haluszczak, C. et al. The antigen-specific  $CD8^+$  T cell repertoire in unimmunized mice includes memory phenotype cells bearing markers of homeostatic expansion. *J. Exp. Med.* **206**, 435–448 (2009).
- Chiu, B. -C., Martin, B. E., Stolberg, V. R. & Chensue, S. W. Cutting edge: central memory  $CD8$  T cells in aged mice are virtual memory cells. *J. Immunol.* **191**, 5793–5796 (2013).
- White, J. T., Cross, E. W. & Kedl, R. M. Antigen-inexperienced memory  $CD8^+$  T cells: where they come from and why we need them. *Nat. Rev. Immunol.* **17**, 391–400 (2017).
- Lee, J. Y., Hamilton, S. E., Akue, A. D., Hogquist, K. A. & Jameson, S. C. Virtual memory  $CD8$  T cells display unique functional properties. *Proc. Natl Acad. Sci. USA* **110**, 13498–13503 (2013).
- Quinn, K. M. et al. Age-related decline in primary  $CD8^+$  T cell responses is associated with the development of senescence in virtual memory  $CD8^+$  T cells. *Cell Rep.* **23**, 3512–3524 (2018).
- Sosinowski, T. et al.  $CD8\alpha^+$  dendritic cell trans presentation of IL-15 to naive  $CD8^+$  T cells produces antigen-inexperienced T cells in the periphery with memory phenotype and function. *J. Immunol.* **190**, 1936–1947 (2013).
- White, J. et al. Virtual memory T cells develop and mediate bystander protective immunity in an IL-15-dependent manner. *Nat. Commun.* **7**, 11291 (2016).
- Rolot, M. et al. Helminth-induced IL-4 expands bystander memory  $CD8^+$  T cells for early control of viral infection. *Nat. Commun.* **9**, 4516 (2018).
- Lin, J. S. et al. Virtual memory  $CD8$  T cells expanded by helminth infection confer broad protection against bacterial infection. *Mucosal Immunol.* **12**, 258–264 (2019).
- Jin, J. H. et al. Virtual memory  $CD8^+$  T cells restrain the viral reservoir in HIV-1-infected patients with antiretroviral therapy through derepressing KIR-mediated inhibition. *Cell. Mol. Immunol.* **17**, 1257–1265 (2020).
- Miller, C. H. et al. Eomes identifies thymic precursors of self-specific memory-phenotype  $CD8^+$  T cells. *Nat. Immunol.* **21**, 567–577 (2020).
- Wang, X. et al. MHC class I-independent activation of virtual memory  $CD8$  T cells induced by chemotherapeutic agent-treated cancer cells. *Cell. Mol. Immunol.* <https://doi.org/10.1038/s41423-020-0463-2> (2020).
- McElwce, K. J., Boggess, D., King, J. & Sundberg, J. P. Experimental induction of alopecia areata-like hair loss in C3H/HeJ mice using a full-thickness skin grafts. *J. Invest. Dermatol.* **111**, 797–803 (1998).
- Pratt, C. H., King, L. E., Messenger, A. G., Christiano, A. M. & Sundberg, J. P. Alopecia areata. *Nat. Rev. Dis. Prim.* **3**, 1–17 (2017).

15. Xing, L. et al. Alopecia areata is driven by cytotoxic T lymphocytes and is reversed by JAK inhibition. *Nat. Med.* **20**, 1043–1049 (2014).
16. Qiu, X. et al. Reversed graph embedding resolves complex single-cell trajectories. *Nat. Methods* **14**, 979–982 (2017).
17. Becker, J. C., Varki, N., Bröcker, E. B. & Reisfeld, R. A. Lymphocyte-mediated alopecia in C57BL/6 mice following successful immunotherapy for melanoma. *J. Invest. Dermatol.* **107**, 627–632 (1996).
18. Gilhar, A. et al. Melanocyte-associated T cell epitopes can function as autoantigens for transfer of alopecia areata to human scalp explants on Prkdc(scid) mice. *J. Invest. Dermatol.* **117**, 1357–1362 (2001).
19. Wang, E. H. C. et al. Identification of autoantigen epitopes in alopecia areata. *J. Invest. Dermatol.* **136**, 1617–1626 (2016).
20. Chu, T. et al. Bystander-activated memory CD8 T cells control early pathogen load in an innate-like, NKG2D-dependent manner. *Cell Rep.* **3**, 701–708 (2013).
21. Ashouri, J. F. & Weiss, A. Endogenous Nur77 is a specific indicator of antigen receptor signaling in human T and B cells. *J. Immunol.* **198**, 657–668 (2017).
22. Borchering, N. et al. A transcriptomic map of murine and human alopecia areata. *JCI Insight* **5**, e137424 (2020).
23. Jacomet, F. et al. Evidence for eomesodermin-expressing innate-like CD8<sup>+</sup> KIR/NKG2A<sup>+</sup> T cells in human adults and cord blood samples. *Eur. J. Immunol.* **45**, 1926–1933 (2015).
24. Mackay, L. K. et al. The developmental pathway for CD103<sup>+</sup>CD8<sup>+</sup> tissue-resident memory T cells of skin. *Nat. Immunol.* **14**, 1294–1301 (2013).
25. Petukhova, L. et al. Genome-wide association study in alopecia areata implicates both innate and adaptive immunity. *Nature* **466**, 113–117 (2010).
26. Lee, S., Lee, H., Lee, C. H. & Lee, W. S. Comorbidities in alopecia areata: a systematic review and meta-analysis. *J. Am. Acad. Dermatol.* **80**, 466–477 (2019).
27. Egeberg, A., Anderson, S., Edson-Heredia, E. & Burge, R. Comorbidities of alopecia areata: a population-based cohort study. *Clin. Exp. Dermatol.* **46**, 651–656 (2021).
28. Shin, J. W. et al. Time-dependent risk of acute myocardial infarction in patients with alopecia areata in Korea. *JAMA Dermatol.* **156**, 763–771 (2020).
29. McPhee, C. G. et al. Increased expression of Cxcr3 and its ligands, Cxcl9 and Cxcl10, during the development of alopecia areata in the mouse. *J. Invest. Dermatol.* **132**, 1736–1738 (2012).
30. Dai, Z. et al. CXCR3 blockade inhibits T cell migration into the skin and prevents development of alopecia areata. *J. Immunol.* **197**, 1089–1099 (2016).

**Publisher's note** Springer Nature remains neutral with regard to jurisdictional claims in published maps and institutional affiliations.

Springer Nature or its licensor (e.g. a society or other partner) holds exclusive rights to this article under a publishing agreement with the author(s) or other rightsholder(s); author self-archiving of the accepted manuscript version of this article is solely governed by the terms of such publishing agreement and applicable law.

© The Author(s), under exclusive licence to Springer Nature America, Inc. 2023

## Methods

### Mice

Experiments were performed using 8- to 16-week-old female C3H/HeJ (Jackson Laboratories), BALB/c and C57BL/6J (DBL) mice in compliance with institutional guidelines as approved by the Institutional Animal Care and Use Committee of Korea Advanced Institute of Science and Technology (KA2019-55). Mice were provided a solid diet (Envigo, 2018C) throughout the experimental period, allowing them to freely consume. The mice were acclimated for 1 week under controlled conditions of temperature ( $23 \pm 2^\circ\text{C}$ ), humidity ( $55\% \pm 10\%$ ), and a 12-h light–dark cycle before being used for the subsequent experiments. No statistical methods were used to predetermine sample sizes, but our sample sizes are similar to those reported in previous publications<sup>15,30</sup>. Age-matched mice were randomly allocated. Data collection and analysis were not performed blind to the conditions of the experiments. No data points or mice were excluded for analysis in this study.

### Induction of alopecia areata in C3H/HeJ mice

Since AA spontaneously occurs in C3H/HeJ mice at a very low frequency ( $\sim 0.25\%$  in 5-month-old C3H/HeJ mice and  $<20\%$  in 18-month-old mice), AA mice derived from AT have been widely used for AA research. In the current study, we utilized AA mice derived from AT as well as mice with spontaneously developed AA, and found that the phenotypic and functional characteristics of CD44<sup>5hi</sup>CD49d<sup>lo</sup> CD8<sup>+</sup> T cells did not differ between SpAA and AtAA mice (Figs. 1b,d,i–k, 3c,d and 4b–d,f and Supplementary Fig. 6a). To control AA onset and increase the number of AA-affected mice, we transferred cultured lymph node-derived cells from the SDLNs of AA-affected mice, as previously reported<sup>31</sup>. Single-cell suspensions of lymph nodes were prepared and cultured for 6 days with  $30 \text{ U ml}^{-1}$  IL-2 (Roche Life Science),  $25 \text{ ng ml}^{-1}$  IL-7 (R&D Systems, Minneapolis, MN),  $50 \text{ ng ml}^{-1}$  IL-15 (R&D Systems) and Mouse T-Activator CD3/CD28 Dynabeads (Invitrogen) to increase lymph node counts 8-fold to 10-fold, as previously described. The cultured cells ( $1\text{--}2 \times 10^7$ ) were injected into naive C3H/HeJ mice intradermally. TCR engagement by 'Mouse T-Activator CD3/CD28 Dynabeads' during *in vitro* culture before AT do not affect the generation of CD44<sup>5hi</sup>CD49d<sup>lo</sup> CD8<sup>+</sup> T cells and do not change the disease-free ratio after AT (Supplementary Fig. 9a–g).

### Adoptive transfer of T cells into C3H/HeJ mice

Single-cell suspensions were prepared from SDLNs obtained from C3H/HeJ alopecic mice or naive mice. To specify T cell populations, these suspensions were stained with anti-CD3, anti-CD8, anti-CD44 and anti-CD49d, and then sorted to obtain the following fractions: AA CD44<sup>5hi</sup>CD49d<sup>lo</sup> cells, AA T<sub>VM</sub> cells and naive T<sub>VM</sub> cells (FACS Aria II cell sorter; BD Biosciences). We next intradermally injected  $1 \times 10^5$  sorted cells of each population into 10-week-old C3H/HeJ mice.

For *in vivo* experiments with cytokine-stimulated cells, T<sub>VM</sub> and T<sub>N</sub> cells from naive mice were sorted using a FACS Aria II cell sorter, and then cultured for 6 days with  $30 \text{ U ml}^{-1}$  IL-2 (Roche),  $25 \text{ ng ml}^{-1}$  IL-7 (R&D Systems),  $50 \text{ ng ml}^{-1}$  IL-15 (R&D Systems),  $50 \text{ ng ml}^{-1}$  IL-12 (R&D Systems) and  $50 \text{ ng ml}^{-1}$  IL-18 (R&D Systems). Finally, the cultured cells ( $1 \times 10^5$ ) were intradermally injected into 10-week-old C3H/HeJ mice.

### Viral infection

C3H/HeJ female mice were anesthetized with Zoletil 50 (tiletamine  $125 \text{ mg}$ , zolazepam  $125 \text{ mg}$   $5 \text{ ml}^{-1}$ ) and Rompun (xylazine), and then infected with various viruses. Naive C3H/HeJ mice were intraperitoneally injected with  $1 \times 10^6$  plaque-forming units (PFUs) of MCMV or intranasally administered 10 PFUs of A/Puerto Rico/8/1934 (PR8). Mice infected with MCMV or IAV were euthanized 4 weeks after infection. Cells were isolated from the SDLNs, spleen and skin, and were used for flow cytometry or ELISpot analyses.

VV infection was performed via skin scarification with  $3 \times 10^6$  PFUs using a previously described scarification method<sup>32,33</sup>. Briefly,  $30 \mu\text{l}$  of

VV was applied to the shaved dorsal side of mice (an area of  $3\text{--}5 \text{ cm}^2$ ), and then the skin was gently scratched 50 times with a 27-gauge needle. VV infection in the skin was evident based on the significant increase of CD44<sup>+</sup>CD49d<sup>+</sup> cells in the skin and SDLNs (Extended Data Fig. 4a–c) as well as the skin scabbing at 1 week after VV infection. At 4 weeks after infection, the infected mice were injected with cultured lymph node-derived cells obtained from the SDLNs of AA-affected mice, to confirm the role of antigen-experienced memory T cells.

### Production of influenza A virus PR8 HA<sub>352–60</sub>-specific dextramer

Naive C3H mice were infected with IAV (PR8) to generate antigen-primed memory CD8<sup>+</sup> T cells. The minimal epitope sequence (HA<sub>352–360</sub>, IEGGWTGMI) for high-affinity binding to mouse MHC class I, H-2K<sup>k</sup>, was identified using *in silico* NetMHC 4.0 analysis and IFN $\gamma$  ELISpot assays (Mabtech). ELISpot was performed using the ELISpot Plus: Mouse IFN $\gamma$  (ALP) kit (Mabtech). Splenocytes from IAV-infected mice were cultured in RPMI/10% FBS with individual peptides ( $1 \text{ mg ml}^{-1}$  with 5% dimethyl sulfoxide) at a final concentration of  $10 \text{ mg ml}^{-1}$ . Dimethyl sulfoxide (0.05%) was used as a negative control, and phorbol 12-myristate 13-acetate plus ionomycin as a positive control. After a 24-h incubation at  $37^\circ\text{C}$ , the spots were developed following the manufacturer's instructions. Spots were counted using an ELISpot reader (CTL; ImmunoSpot), and the number of specific spots was calculated by subtracting the number of spots in negative control wells from the number in peptide-stimulated wells. After identifying HA<sub>352–60</sub> as an epitope candidate, we obtained PE-conjugated Dextramer reagent from Immudex. For Dextramer staining, cells were incubated with PE-conjugated Dextramer (IEGGWTGMI) at room temperature (RT) for 30 min in the presence of anti-mouse CD16/32 (2.4G2; BD Biosciences).

### Retroviral transduction of mouse T cells

To track the adoptively transferred T<sub>VM</sub> cells from AA, we used a retroviral GFP transduction method. SDLNs were obtained from AA mice and subjected to single-cell isolation. Among the isolated SDLN cells, the T<sub>VM</sub> cells were sorted using a FACS Aria II (BD Biosciences). Next, the AA T<sub>VM</sub> cells were cultured with  $100 \text{ U ml}^{-1}$  IL-2 (Roche),  $25 \text{ ng ml}^{-1}$  IL-7 (R&D Systems),  $50 \text{ ng ml}^{-1}$  IL-15 (R&D Systems) and CD3/CD28 Dynabeads for 24 h in RPMI1640/10%. At 24 h after activation,  $500 \mu\text{l}$  of GFP retrovirus supernatant was added to a 24-well non-tissue culture plate that was pre-coated with  $20 \mu\text{g ml}^{-1}$  RetroNectin (Takara). We next centrifuged the plate at  $2,000\text{g}$  for 2 h at  $32^\circ\text{C}$ . The activated T<sub>VM</sub> cells ( $1 \times 10^6$  cells in  $500 \mu\text{l}$  media) were transferred into the plate without suction (final volume of 1 ml). Next, the T<sub>VM</sub> cells were spin-transduced at  $1,000\text{g}$  for 10 min at  $32^\circ\text{C}$ , and the plate was placed in the CO<sub>2</sub> incubator at  $37^\circ\text{C}$  for 2 days. At 2 days after transduction, we suctioned out  $400 \mu\text{l}$  of media, and then added  $500 \mu\text{l}$  of the previously described RPMI1640/FBS 10% media with IL-2, IL-7 and IL-15. At 4 days after transduction, the cells were spun down and Dynabeads were removed. For *in vivo* experiments, the GFP-expressing retrovirus-transduced T<sub>VM</sub> cells were intradermally injected into naive C3H/HeJ mice.

### Human samples

The study population comprised ten individuals with AA who had ceased treatment for 3 months, and ten healthy volunteers (Supplementary Table 4). This study was approved by the Institutional Review Board of Chung-Ang University Hospital (approval no. CAU-DERMA-AA01). Informed consent was obtained from all participants.

### Single-cell isolation

To prepare a single-cell suspension of mouse skin, fat was removed from the overlying skin in PBS. Then, the skin was incubated in collagenase type I ( $2 \text{ mg ml}^{-1}$  in PBS) at  $37^\circ\text{C}$  for 75 min. After digestion, the skin was minced in RPMI/10% FBS, filtered through a  $70\text{-}\mu\text{m}$  cell strainer, and centrifuged at  $300\text{g}$  for 7 min. Then, the pellet was resuspended in

RPMI/10% FBS, filtered through a 70- $\mu$ m cell strainer and centrifuged at 300 g for 7 min. SDLNs were pooled, minced in RPMI/10% FBS, filtered through a 70- $\mu$ m cell strainer and centrifuged at 300g for 7 min. The spleen and the liver were minced through a 70- $\mu$ m cell strainer, and the dissected pellets were incubated with red blood cell lysis buffer at RT for 5 min. All single-cell suspensions were additionally processed for the indicated analyses.

Peripheral blood mononuclear cells were isolated from whole human blood by standard Ficoll-Paque (GE Healthcare) density gradient centrifugation. Purified lymphocytes were cryopreserved until use.

### Antibodies for flow cytometry

Mouse studies were performed using the following antibodies: anti-CD3 (17A2; BioLegend), anti-CD8 (53-6.7; BD Biosciences), anti-CD44 (IM7; BD Biosciences), anti-CD49d (R1-2; BioLegend), anti-CD62L (MEL-14; BD Biosciences), anti-NKG2D (CX5; BioLegend), anti-Gzmb (QA16A02; BioLegend), anti-Perforin (S16009A; BioLegend), anti-IFN $\gamma$  (XMG1.2; BD Biosciences), anti-TNF (MP6-XT22; BD Biosciences), anti-Ki-67 (B56; BD Biosciences), anti-Nur77 (12.14; Invitrogen), anti-TCR $\beta$  (H57-597; BioLegend), anti-TCR $\gamma\delta$  (GL3; BD Biosciences), anti-CD19 (1D3; BD Biosciences), anti-CD14 (rmC5-3; BD Biosciences), anti-CD103 (M290; BD Biosciences) and anti-CD49a (HM $\alpha$ 1; BioLegend).

Human studies were performed using the following antibodies: anti-CD3 (UCHT-1; BD Biosciences), anti-CD8 (SK1; BD Biosciences), anti-CD161 (DX12; BD Biosciences), anti-CD45RA (HI100; BioLegend), anti-CD27 (M-T271; BD Biosciences), anti-KIR2D (REA1042; Miltenyi Biotec), anti-KIR3DL1/DL2 (REA970; Miltenyi Biotec), anti-NKG2A (REA110; Miltenyi Biotec) and anti-NKG2D (1D11; BioLegend).

### Measurement of cytokine production and proliferative capacity

To detect the ex vivo production of functional cytokines and intracellular molecules without any stimulation, single-cell suspensions isolated from skin and SDLNs were incubated with GolgiPlug (BD Biosciences) and GolgiStop (BD Biosciences) at 37 °C for 5 h without stimulation. First, the single-cell suspensions were incubated with anti-CD16/CD32 (93; BioLegend) for 20 min at 4 °C to block the nonspecific binding of antibodies to Fc $\gamma$ R. Next, the cells were stained using the LIVE/DEAD fixable dead cell stain kit (Invitrogen) and antibodies for cell surface molecules at RT for 30 min. After washing, the stained cells were fixed and permeabilized using a forkhead box protein P3 staining buffer kit (eBioscience). Flow cytometry was performed using an LSR II instrument and FACSDiva software (BD Biosciences). Data were analyzed using FlowJo v10 software (Treestar).

For intracellular staining, the single-cell suspensions from SDLNs were stimulated for 48 h with 50 ng ml<sup>-1</sup> of cytokines (IL-2, IL-7, IL-12 p70, IL-15–IL-15R complex and IL-18). For the last 12 h of incubation, Golgi-Plug and GolgiStop were added to the culture media to stain intracellular molecules. To stain intracellular proteins, surface-marker-stained cells were permeabilized using a Foxp3 staining buffer kit (eBioscience) and further stained for intracellular proteins for 30 min at 4 °C. To assess the proliferation capacity of each cell population, the single-cell suspensions from SDLNs were labeled with CellTrace Violet (Invitrogen) and co-cultured for 72 h with 50 ng ml<sup>-1</sup> of cytokines (IL-2, IL-7, IL-12 p70, IL-15–IL-15R complex and IL-18).

### In vivo blockade of NKG2D and cytokines

For prevention studies, mice were administered treatment starting on the day of AT. Mice received an intraperitoneal injection of monoclonal anti-NKG2D (200  $\mu$ g in 100  $\mu$ l; HMG-2D; BioXCell), monoclonal anti-IL-12 (500  $\mu$ g in 100  $\mu$ l; R2-9A5; BioXCell), anti-IL-15 monoclonal antibody (200  $\mu$ g in 100  $\mu$ l; TM- $\beta$ 1; BioLegend), anti-IL-18 monoclonal antibody (200  $\mu$ g in 100  $\mu$ l; YIGIF74-1G7; BioXCell) or control rat IgG (200  $\mu$ g in 100  $\mu$ l PBS; LTF-2; BioXCell) two times weekly for 12 weeks. Hair status was examined twice weekly.

### In vitro lactate dehydrogenase release assay

Lactate dehydrogenase (LDH) release assay to measure cytotoxicity was performed using the following effector cells: AA CD44<sup>s-hi</sup> cells, AA T<sub>VM</sub> cells and AA T<sub>N</sub> cells sorted from SDLNs. These effector cells were co-cultured at a 20:1 E:T ratio with YAC-1 cells (which express NKG-2DLs, such as H60 and Rae-1) as target cells. For the blocking experiment, before YAC-1 exposure, the effector cells were pre-incubated for 30 min with 10  $\mu$ g ml<sup>-1</sup> anti-NKG2D (HMG-2D; BioXCell) or isotype antibody (LTF-2; BioXCell). YAC-1 cells co-cultured with different effector cells were incubated for 24 h at 37 °C and 5% CO<sub>2</sub>. LDH activity in the cell supernatants was assessed using an LDH Cytotoxicity Assay Kit II (ab65393; Abcam).

### ELISA

The mice were euthanized using CO<sub>2</sub> overdose, and their skin was collected and washed twice with 1 ml PBS. Next, 0.2-mg samples of skin were collected and homogenized using a Precellys 24 tissue homogenizer and beads (Bertin Instruments) for skin lysates. The indicated cytokines were detected by sandwich ELISA, and the concentrations were calculated by standard curves using the IL-12, IL-15–IL-15R complex and IL-18 ELISA kits (Invitrogen) with duplicated samples.

### Quantitative real-time PCR

To measure the expression levels of *Nr4a1*, *Nr4a2* and *Nr4a3*, mice were euthanized at 4, 6 and 8 weeks after AT, and total RNA was extracted from CD44<sup>s-hi</sup>CD49d<sup>lo</sup> CD8<sup>+</sup> T cells using TRIzol reagent, according to the manufacturer's instructions. The first complementary DNA (cDNA) strand of the entire RNA template was synthesized using Prime Script RT Master Mix (Takara). The mRNA expression was quantified using qPCR 2X PreMIX SYBR (Enzynomics) and normalized to the housekeeping gene *GAPDH* using a CFX-96 thermocycler (Bio-Rad). We calculated the fold change in expression using the comparative CT method ( $\Delta\Delta C_T$  method). The following primers were used: *GAPDH*-F, GAAGTCGGTGTGAACGGA; *GAPDH*-R, GTTAGTGGGGTCTCGCTCCT<sup>15</sup>; *Nr4a1*-F, TGTGAGGCTGCAAGGGCTTC; *Nr4a1*-R, AAGCGGCAGAACTGGCAGCGG; *Nr4a2*-F, CTGTGCGCTGTTTGCCTGAC; *Nr4a2*-R, CGGCGCTTGTCTACTGGGCAG; *Nr4a3*-F, AGGGCTTCTCAAGAGAACGG; and *Nr4a3*-R, CCATCCCGACACTGAGACAC<sup>34</sup>.

### Immunofluorescence analysis and immunohistochemistry

For immunofluorescence studies of mouse skin, skin tissues from the abdominal region were fixed with 4% paraformaldehyde in PBS, and then cryoprotected in 30% sucrose in PBS at 4 °C overnight with rotating. Fixed tissues were embedded in OCT compound, and embedded skin tissues were sectioned sagittally (15- $\mu$ m-thick) on a Leica CM1850 cryostat. Skin tissues were blocked and permeabilized with blocking solution (5% normal donkey serum, 3% BSA and 0.1% Triton X-100 in 0.1 M PBS) for 1 h at RT, followed by overnight incubation at 4 °C with primary antibodies diluted in the blocking solution. Tissues were immunostained using the following antibodies: anti-IL-12 (Invitrogen, 9A5, MMI20), anti-IL-15 (R&D systems, polyclonal, AF447), anti-IL-18 (Abcam, EPR22249-212, ab223293), anti-CD45 (R&D systems, polyclonal, AF114) and anti-CK14 (Abcam, ERP17350, ab181595). After washing, secondary antibodies diluted in blocking solution were applied to the sections for 1 h at RT in the dark. Secondary antibodies were Alexa Fluor 488-, Alexa Fluor 594- or Alexa Fluor 647-conjugated donkey anti-rat, donkey anti-rabbit and donkey anti-goat (Jackson ImmunoResearch). Nuclei were visualized by incubation for 15 min with 10  $\mu$ g ml<sup>-1</sup> trihydrochloride (Hoechst 33342, Invitrogen) in 0.1 M PBS. Stained sections were mounted with 2.5% PVA/DABCO mounting media and analyzed.

For immunofluorescence studies of human skin, 5  $\mu$ M formalin-fixed and paraffin-embedded skin sections were used. After heat-induced antigen retrieval with sodium citrate solution (pH 6.0) or Tris-EDTA solution (pH 9.0) at 95 °C for 20 min, and then 20 °C for

20 min, skin sections were stained following the same protocol as for mouse skin tissue but using the following primary anti-human antibodies: anti-IL-12 (Abcam, polyclonal, ab124635), anti-IL-15 (Abcam, 3A3, ab55276), anti-IL-18 (Abcam, polyclonal, ab191152), anti-CD8 (Bio-Rad, YTC182.20, MCA351G), anti-NG2A (R&D Systems, 131411, MAB1059-100) and anti-KIR2DL (Abcam, EPR22492-64, ab255327). Secondary antibodies were Alexa Fluor 488-, Alexa Fluor 594-, or Alexa Fluor 647-conjugated donkey anti-rat, donkey anti-rabbit, donkey anti-mouse and donkey anti-goat (Jackson ImmunoResearch). All images were captured using an A1 HD25 Nikon confocal microscope.

For immunohistochemistry studies of mouse skin, 10% neutral buffered formalin-fixed and paraffin-embedded skin sections with a thickness of 5  $\mu$ m were used. The lesion area of the test animal tissue was fixed in 10% neutral buffered formalin at the end of the experiment. After step-by-step dehydration using ethanol solution (starting from a low concentration to high concentration), paraffin blocks were prepared. Each tissue block was cut to a thickness of 5  $\mu$ m for attachment to the slide, and each tissue slide was deparaffinized with xylene and dehydrated using ethanol. After the deparaffinization and rehydration step, antigen retrieval was carried out for 15 min at 90 °C using Tris-EDTA HIER Solution (pH 9.0; Scytek Laboratories, TES999) and a water bath. Skin tissues were blocked using BLOXALL Endogenous Blocking Solution (Vector Laboratories, SP-6000) for 10 min at RT. Primary staining and DAB staining was performed using the ImmPRESS horseradish peroxidase horse anti-goat IgG polymer detection kit (Vector Laboratories, MP-7405), antibody diluent solution (GBI Labs, E09-300) and anti-Rae-1 (R&D systems, polyclonal, AF1136) according to the manufacturer's recommendations. After washing, DAB staining was performed using the ImmPACT DAB Substrate (Vector Laboratories, SK-4105) according to the manufacturer's recommendations. Stained sections were dehydrated and mounted in MM 24 mounting media (Leica, 3801120). All stained mouse tissue slides were imaged using a slide scanner (Pannoramic MIDI; 3DHISTECH) and observed using Case Viewer software.

### Bulk RNA-seq and transcriptome analysis

Skin and SDLN single-cell suspensions were generated by pooling samples from three or four mice. Total CD8<sup>+</sup> T cells were sorted using a CD8 $\alpha$ <sup>+</sup> T cell isolation kit (Miltenyi Biotec), and AA cells were enriched using a FACS Aria II cell sorter. All sorted samples had >97% purity, and QuantSeq 3' mRNA sequencing was performed. The RNA was extracted from sorted cells preserved in TRIzol reagent (Invitrogen) and quality assessed using the 2100 Bioanalyzer System (Agilent). Library generation and amplification were performed using the QuantSeq 3' mRNA-Seq Library Prep Kit (Lexogen). Single-end 75-bp sequencing was performed using Illumina NextSeq 500. After trimming at cutoff Q20 using BBduk, the sequences were aligned to the mm10 mouse reference genome from UCSC using Bowtie2. The read counts were calculated by Bedtools and normalized using DESeq2 (version 1.26.0) considering the sequencing depth and gene composition. Differentially expressed genes were selected according to cutoff adjusted *P* values < 0.05 and  $|\log_2 \text{fold change}| > 2$ . GSEA was performed using clusterProfiler with GO biological process gene sets, immunological signatures from MSigDB, and the specific gene sets from BIOCARTA\_TCR\_PATHWAY, T<sub>RM</sub> gene set<sup>24</sup> and GOLDRATH\_EFF\_VS\_MEMORY\_CD8\_T\_CELL<sup>35</sup>.

### TCR sequencing

The isolated RNA (RNeasy Micro Kit with DNase Treatment, Qiagen) was amplified using a commercially available multiplex primer mix covering the TCR $\beta$  chain (iRepertoire).

Amplified libraries were multiplexed and pooled for sequencing on the Illumina MiSeq platform using a 600-cycle kit and sequenced as 300-bp paired-end reads. The output of the immune receptor sequence covered from within the second framework region through the beginning of the constant region, including complementary determining

region (CDR) 2 and CDR3. Raw sequencing data were analyzed using the iRmap<sup>36,37</sup>. Briefly, sequence reads were de-multiplexed according to Illumina dual indices incorporated during the amplification process and barcode sequences at the 5' ends of reads from the constant region. Next, the reads were trimmed according to their base qualities using a 2-base sliding window. If either quality value in this window was <20, the sequence stretching from the window to the 3' end was trimmed out from the original read. Trimmed pair-end reads were joined together through overlapping alignment using a modified Needleman–Wunsch algorithm. If paired forward and reverse reads in the overlapping region were not perfectly matched, both the forward and reverse reads were thrown out without further consideration. Applying a Smith–Waterman algorithm, the merged reads were mapped to germline V, D, J and C reference sequences using an IMG T reference library. To define the CDR3 region, the positions of the CDR3 boundaries of reference sequences from the IMG T database were migrated onto reads through mapping results, and the resulting CDR3 regions were extracted and translated into amino acids. The clonotype landscape was analyzed using the immunArch R package version 0.6.5 (ref. 38) and iRweb (iRepertoire). To analyze TCR repertoire similarity, we also analyzed CDR3 elements using the Morisita–Horn similarity index.

### CITE-seq

Barcoded single-cell 30 cDNA libraries were generated for each sample pool from FACS-sorted CD45<sup>+</sup> single-cell suspensions from the different samples using the Chromium Single Cell 3' Gel Bead and Library Kit v2 (10x Genomics) following the manufacturer's instructions.

The purified libraries were quantified using qPCR following the qPCR Quantification Protocol Guide (KAPA) and assessed for quality using the Agilent Technologies 4200 TapeStation. Next, the libraries were sequenced using the HiSeqXten platform (Illumina) according to the read length in the user guide. Libraries were constructed and sequenced at a depth of approximately 60,000 reads for each cell. We used the Cell Ranger v3.1.0 (10x Genomics) pipeline to generate FASTQ files from raw sequencing data, for gene expression analysis of 5' gene expression library data, and for cell surface protein expression analysis of the feature barcode libraries. Illumina basecall files from the Illumina sequencing instrument were converted to FASTQ format for each sample using the 'mkfastq' command.

Gene expression and feature barcode libraries were analyzed using the 'count' command. The sequencing reads of gene expression libraries were aligned to the mm10-3.0.0 reference genome using STAR (v2.5.1b) aligner. The reads of the feature barcoded libraries were matched to the target feature barcode reference. Next, gene and cell surface protein expression profiling were performed in each cell using the information on the unique molecular identifier and 10x cell barcode. The cells were then grouped into clusters according to their gene expression.

The following analysis was performed using the Scanpy v1.6.1 package in Python and Seurat package v4.0.2 in R. After generating the feature barcode matrix, we discarded cells that expressed <500 genes and genes that were not expressed in any cells. To exclude low-quality cells from our data, we filtered out the cells expressing mitochondrial genes in >10% of their total gene expression. In addition, using predicted doublet scores calculated with the Scrublet v0.2.3 package in Python, potential doublets were removed. For each cell, the gene expression was normalized based on the total and log-transformed read count. Next, batch correction was performed using Harmony v0.0.5 in Python. With this batch-corrected data, weighted nearest-neighbor analysis by Seurat v4.0.2 in R was executed using both weighted RNA and antibody data to generate clusters. Visualization was achieved using uniform manifold approximation and projection. Dot plots and feature plots were created using Scanpy v1.6.1 in Python. Monocle 2 was used to order and plot cells across the 4,097 cells comprising the clusters of CD8<sup>+</sup> naive T cells, T<sub>VM</sub> cells and Klrk1<sup>+</sup>CD8<sup>+</sup> T cells<sup>16</sup>.

### Statistical analysis

Statistical analyses were performed using GraphPad Prism (version 8) and R software (version 3.6.2; R Foundation for Statistical Computing). All data are the mean  $\pm$  s.d. Significance was assessed using *P* values calculated by the Wilcoxon matched pairs signed-rank test, the Mann–Whitney test and the log-rank (Mantel–Cox) test. Data distribution was assumed to be normal but this was not formally tested.

### Reporting summary

Further information on research design is available in the Nature Portfolio Reporting Summary linked to this article.

### Data availability

RNA-seq data generated in this study have been deposited in the Gene Expression Omnibus under accession code GSE229631. Source data are provided with this paper. All other data that support the findings of this study are present in the article and Supplementary files or are available from the corresponding author (S.-H.P.) upon reasonable request.

### Code availability

All the custom codes used in this study are available from the corresponding author (S.-H.P.) upon reasonable request.

### References

- Wang, E. H. C. et al. Transfer of alopecia areata to C3H/HeJ mice using cultured lymph node-derived cells. *J. Invest. Dermatol.* **135**, 2530–2532 (2015).
- Hirai, T. et al. Competition for active TGF $\beta$  cytokine allows for selective retention of antigen-specific tissue-resident memory T cells in the epidermal niche. *Immunity* **54**, 84–98 (2021).
- Jaing, X. et al. Skin infection generates non-migratory memory CD8<sup>+</sup> T<sub>RM</sub> cells providing global skin immunity. *Nature* **483**, 227–231 (2012).
- Jennings, E. et al. Nr4a1 and Nr4a3 reporter mice are differentially sensitive to T cell receptor signal strength and duration. *Cell Rep.* **33**, 108328 (2020).
- Luckey, C. J. et al. Memory T and memory B cells share a transcriptional program of self-renewal with long-term hematopoietic stem cells. *Proc. Natl Acad. Sci. USA* **103**, 3304–3309 (2006).
- Wang, C. et al. High-throughput sequencing reveals a complex pattern of dynamic interrelationships among human T cell subsets. *Proc. Natl Acad. Sci. USA* **107**, 1518–1523 (2010).
- Yang, X. et al. TCRklass: a new K-string-based algorithm for human and mouse TCR repertoire characterization. *J. Immunol.* **194**, 446–454 (2015).
- ImmunoMind Team. Immunarch: an R package for painless analysis of large-scale immune repertoire data <https://doi.org/10.5281/zenodo.3367200> (2019).

### Acknowledgements

This work was supported by the 2020 Joint Research Project of Institutes of Science and Technology and a grant from the National Research Foundation of Korea (NRF) funded by the Korean government (MSIT; NRF-2022R1A2C3007292 and 2021R1A4A1032094, to S.-H.P.). This work was also supported by the 2022 Basic Research Funds from The Korean Hair Research Society (to J.S.) and by a grant of the MD-PhD/Medical Scientist Training Program through the Korea Health Industry Development Institute (KHIDI), funded by the Ministry of Health & Welfare, Republic of Korea (to S.-D.C.). GFP-expressing retroviral vectors were kindly provided by Y.-M. Kim (KAIST, Daejeon, Korea).

### Author contributions

Study design: J.S., E.-C.S. and S.-H.P.; experiment and data collection: J.S., S.-D.C., J.L., Y.C., S.-Y.K., S.-M.L., S.-H.K., S.J., M.J., H.L., A.R.K. and B.C.; data analysis and interpretation: J.S., S.-D.C., J.L., B.C., S.-J.H., I.J., K.-J.Y., J.-E.P., J.H.K., B.J.K., E.-C.S., and S.-H.P.; writing: J.S., S.-D.C. and S.-H.P. with comments from all authors.

### Competing interests

The authors declare no competing interests.

### Additional information

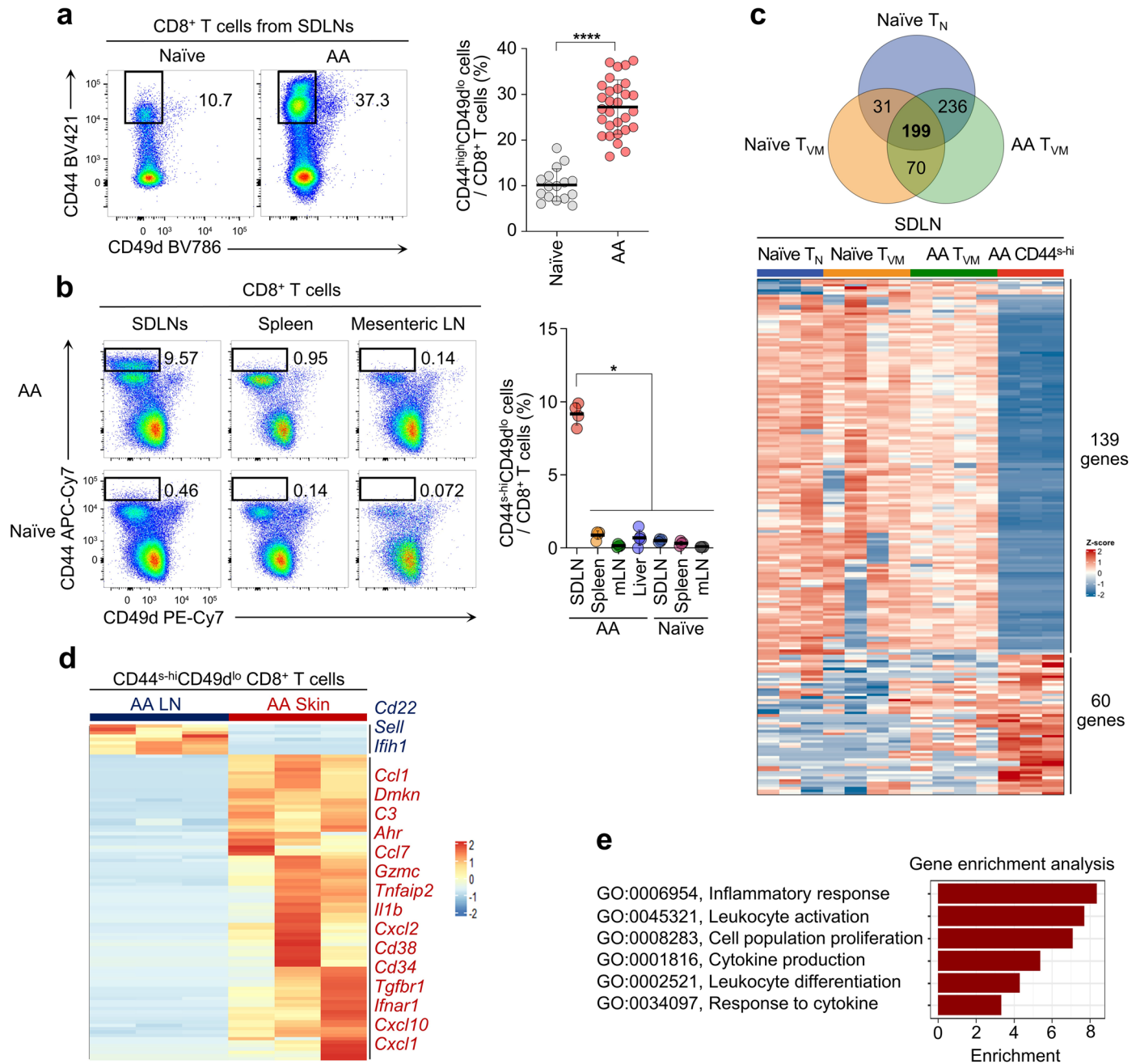
**Extended data** is available for this paper at <https://doi.org/10.1038/s41590-023-01547-5>.

**Supplementary information** The online version contains supplementary material available at <https://doi.org/10.1038/s41590-023-01547-5>.

**Correspondence and requests for materials** should be addressed to Eui-Cheol Shin or Su-Hyung Park.

**Peer review information** *Nature Immunology* thanks Stephen Jameson, Nicole La Gruta, and the other, anonymous, reviewer(s) for their contribution to the peer review of this work. Primary Handling Editor: N. Bernard, in collaboration with the *Nature Immunology* team.

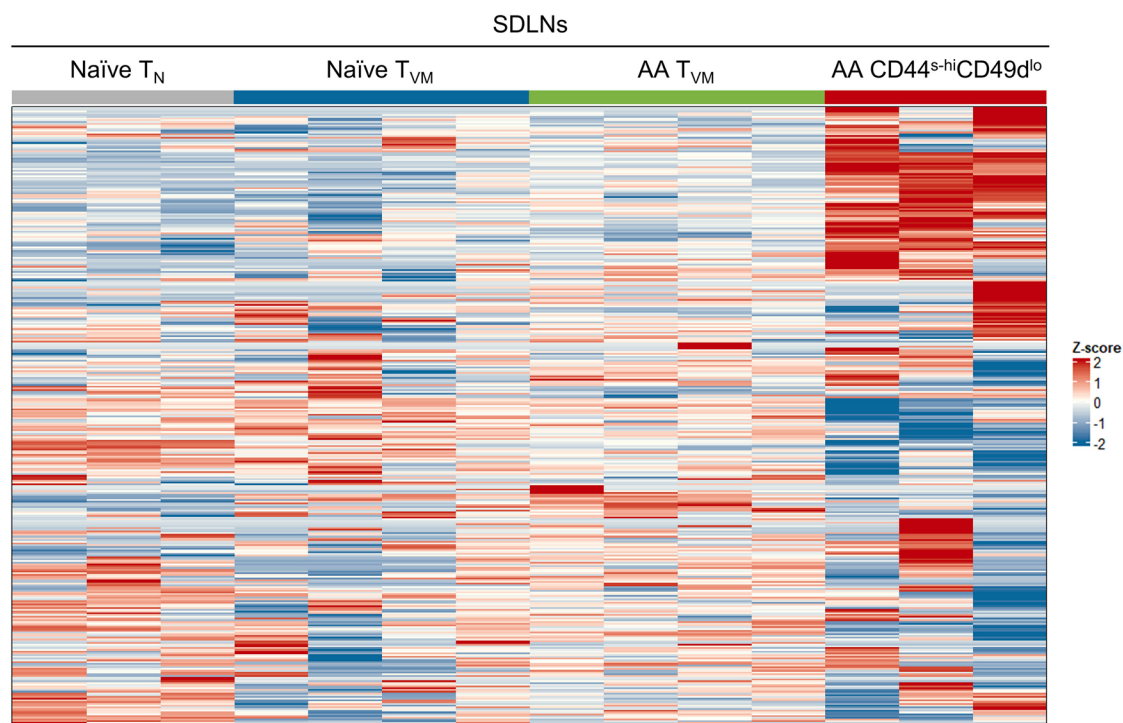
**Reprints and permissions information** is available at [www.nature.com/reprints](http://www.nature.com/reprints).



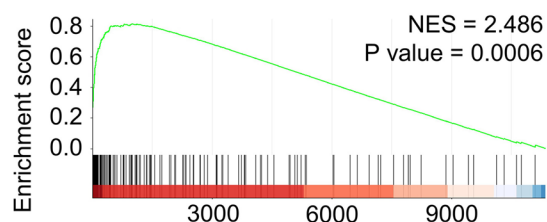
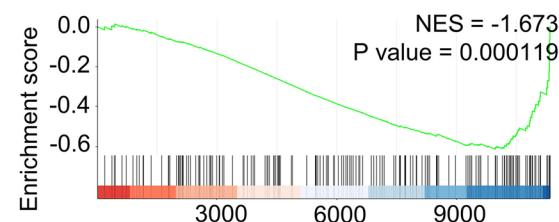
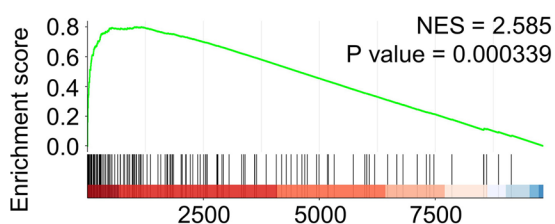
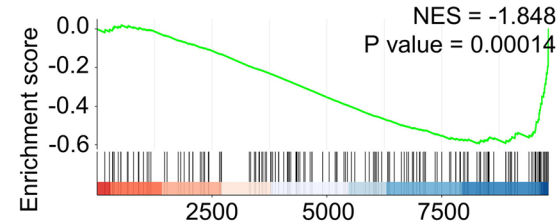
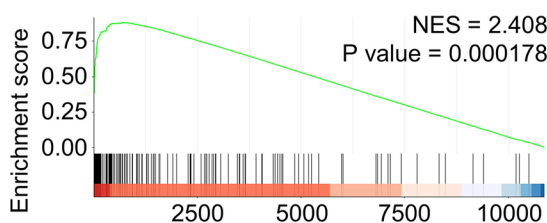
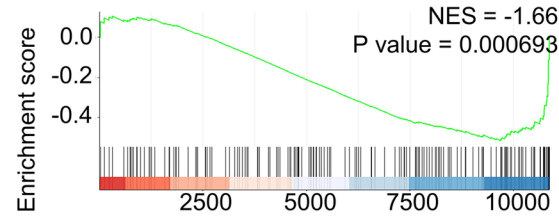
**Extended Data Fig. 1 | CD44<sup>hi</sup>CD49d<sup>lo</sup> CD8<sup>+</sup> T cells are exclusively found in AA SDLNs, and CD44<sup>s-hi</sup>CD49d<sup>lo</sup> CD8<sup>+</sup> T cells from skin exhibit higher expression of genes relevant for cell motility and inflammatory response compared to CD44<sup>hi</sup>CD49d<sup>lo</sup> CD8<sup>+</sup> T cells from SDLNs. a**, The proportion of CD44<sup>high</sup>CD49d<sup>lo</sup> CD8<sup>+</sup> T cells in SDLN CD8<sup>+</sup> T cells ( $n = 16$ , naïve;  $n = 29$ , AA). **b**, CD44<sup>s-hi</sup>CD49d<sup>lo</sup> CD8<sup>+</sup> T cells were nearly absent in the spleens, liver, and skin non-draining mesenteric lymph nodes of alopecic mice ( $n = 5$ , liver;  $n = 4$ , others). **c**, Heatmap of differentially expressed genes (DEGs) in CD44<sup>s-hi</sup>CD49d<sup>lo</sup> CD8<sup>+</sup> T cells from SDLNs relative naïve T<sub>N</sub> cells, naïve T<sub>VM</sub> cells, and AA T<sub>VM</sub>

cells (pairwise comparison). Numbers in overlapping regions indicate gene transcripts shared by the overlapping DEG, whereas numbers in non-overlapping regions indicate unique DEGs to each cell subset. **d**, **e**, Heatmap of DEGs from skin CD44<sup>s-hi</sup>CD49d<sup>lo</sup> CD8<sup>+</sup> T cells compared to SDLN CD44<sup>s-hi</sup>CD49d<sup>lo</sup> CD8<sup>+</sup> T cells (**d**) and enriched GO biological process gene sets (padj < 0.05) (**e**). Data were acquired from AtAA mice. mLN, mesenteric lymph node. Data are presented as mean values ± SD. A Mann-Whitney test was performed for comparisons between two groups. All tests were two sided. \* $P < 0.05$ , \*\*\*\* $P < 0.0001$ .

a



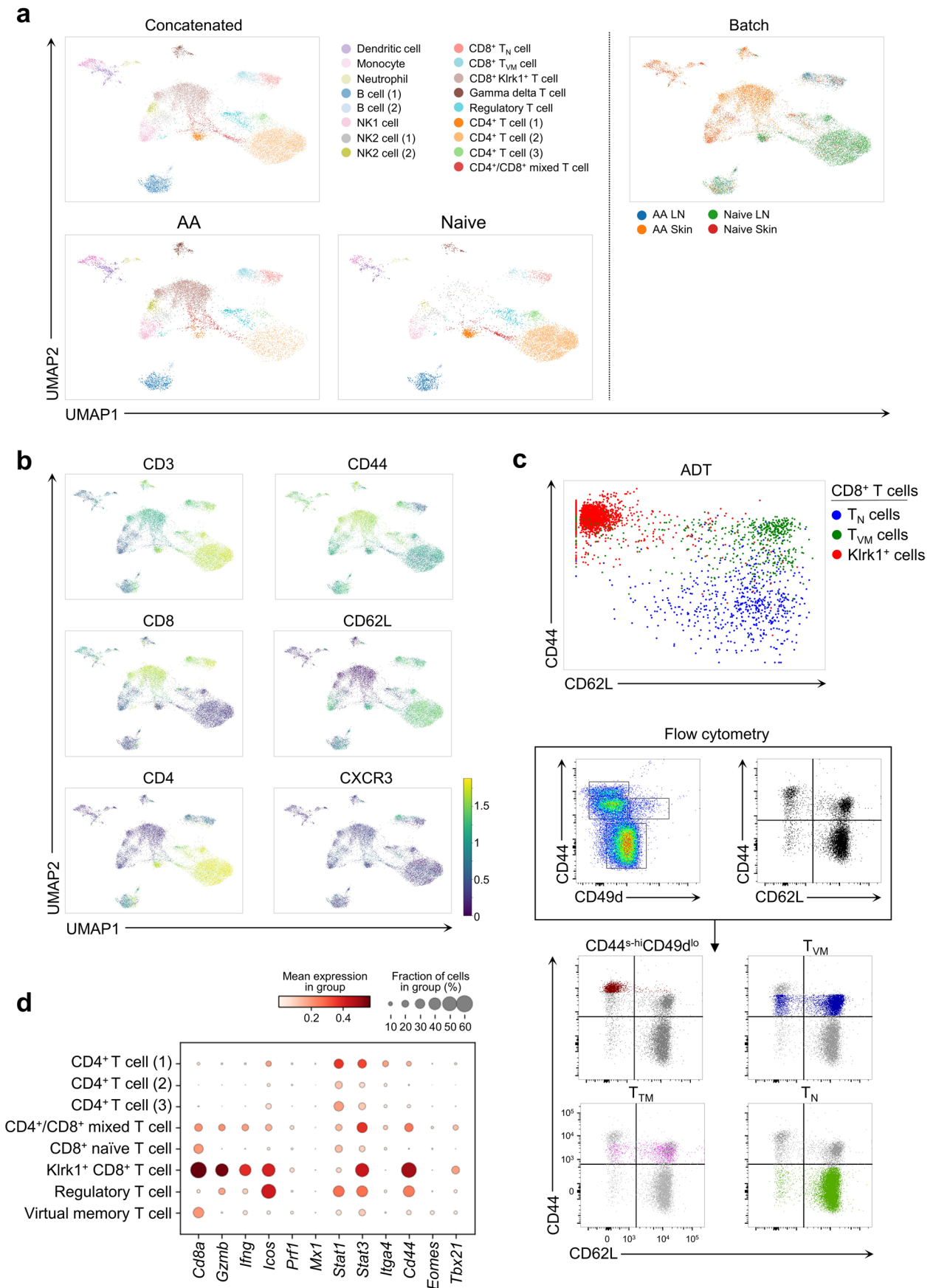
b

**Goldrath gene set**Upregulated (AA LN  $CD44^{s-hi}CD49d^{lo}$  vs. AA LN  $T_{VM}$ )Downregulated (AA LN  $CD44^{s-hi}CD49d^{lo}$  vs. AA LN  $T_{VM}$ )Upregulated (AA LN  $CD44^{s-hi}CD49d^{lo}$  vs. Naive LN  $T_{VM}$ )Downregulated (AA LN  $CD44^{s-hi}CD49d^{lo}$  vs. Naive LN  $T_{VM}$ )Upregulated (AA LN  $CD44^{s-hi}CD49d^{lo}$  vs. Naive LN  $T_N$ )Downregulated (AA LN  $CD44^{s-hi}CD49d^{lo}$  vs. Naive LN  $T_N$ )

**Extended Data Fig. 2 |  $CD44^{s-hi}CD49d^{lo} CD8^+$  T cells had high enrichment of genes related to T-cell effector functions.** a, Heatmap of the gene set<sup>33</sup>. b, GSEA confirmed that  $CD44^{s-hi}CD49d^{lo} CD8^+$  T cells exhibited significant enrichment of the effector  $CD8^+$  T cell gene set<sup>33</sup> compared to  $T_{VM}$  cells from naive or AA mice

and  $T_N$  cells from naive mice. GSEA was performed for pairwise comparison between two groups. All tests were two sided. Data were acquired from AtAA mice. SDLN, skin draining lymph node; NES, normalized enrichment score.

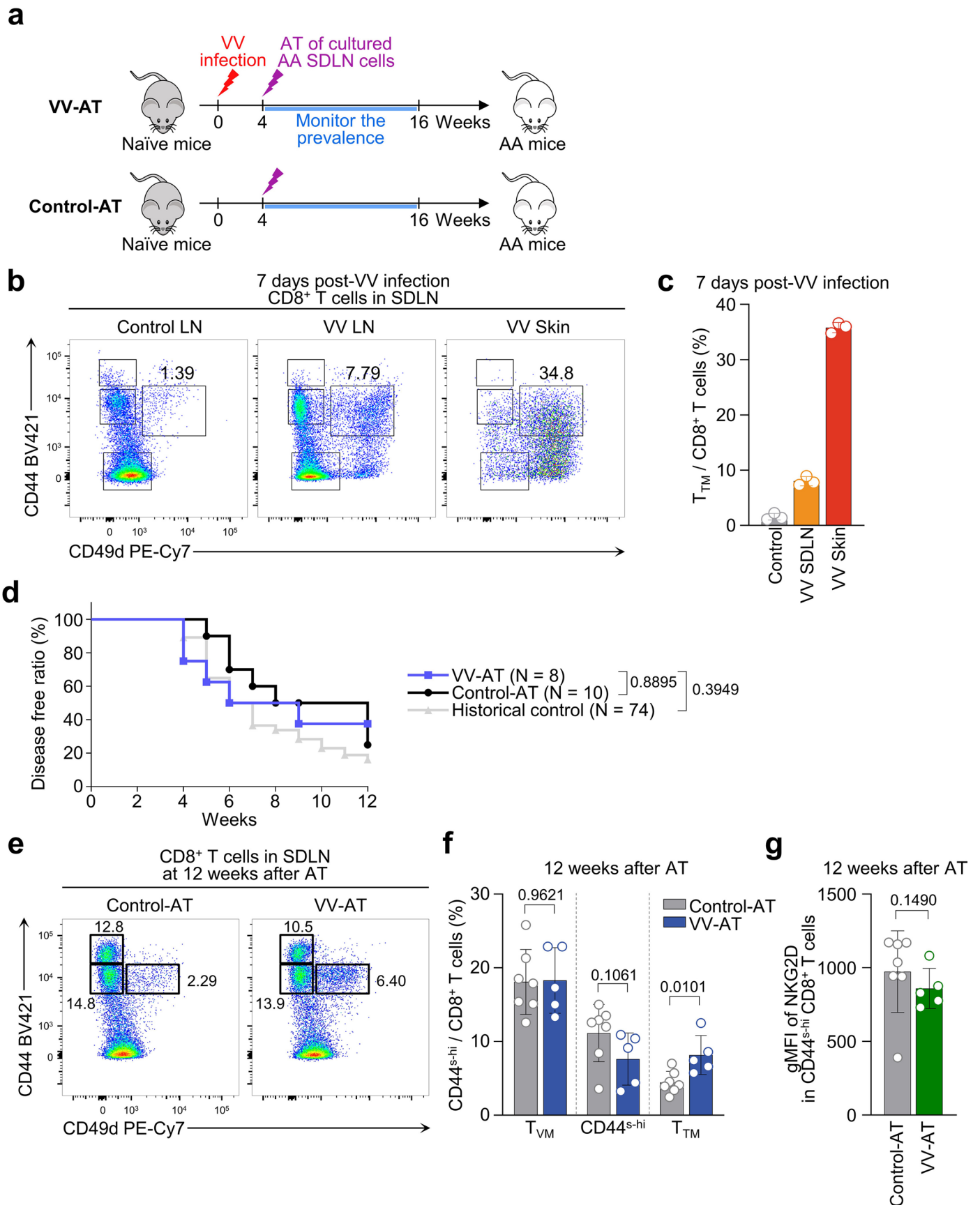




Extended Data Fig. 3 | See next page for caption.

**Extended Data Fig. 3 | Single-cell RNA-seq of CD45<sup>+</sup> cells from the skin and SDLNs of AA and naïve mice.** **a**, UMAP visualization of CD45<sup>+</sup> cell clusters detected in skin and SDLNs from AA and naïve mice. **b**, UMAP visualization of cellular subsets obtained by ADT-labeling of the integrated CITE-Seq. **c**, CD44 and CD62L of ADT-labeling in CD8<sup>+</sup> T cells. Overlays of CD44<sup>s<sup>hi</sup></sup>CD49d<sup>lo</sup> CD8<sup>+</sup> T cells, T<sub>VM</sub> cells, T<sub>TM</sub> cells, and T<sub>N</sub> cells on total CD8<sup>+</sup> T cells with

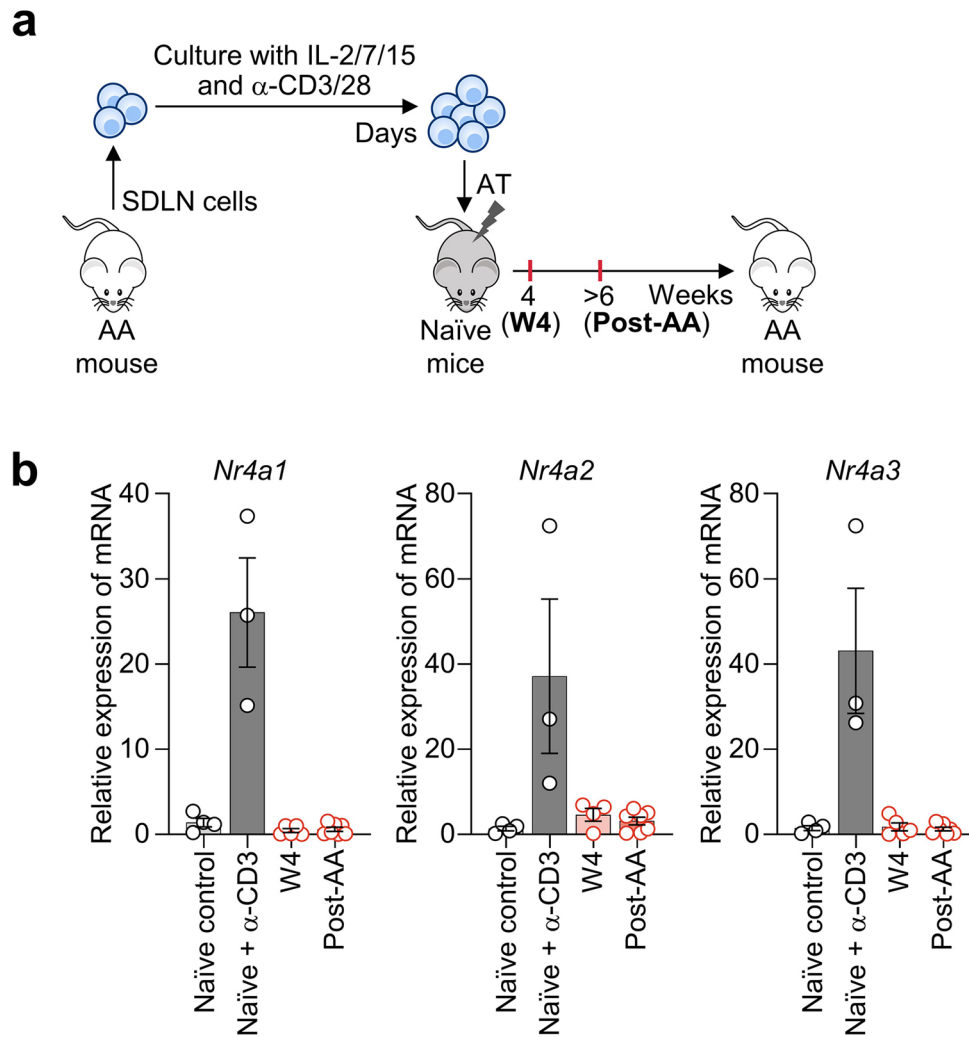
effector memory T cell and central memory T cell gating (CD44<sup>hi</sup>CD62L<sup>lo</sup> and CD44<sup>hi</sup>CD62L<sup>hi</sup>, respectively) in flow cytometric analysis. **d**, Different CD3<sup>+</sup> T-cell clusters and their gene expression levels, with brightness indicating average expression and circle size indicating the percent expression. Data were acquired from AtAA mice.



Extended Data Fig. 4 | See next page for caption.

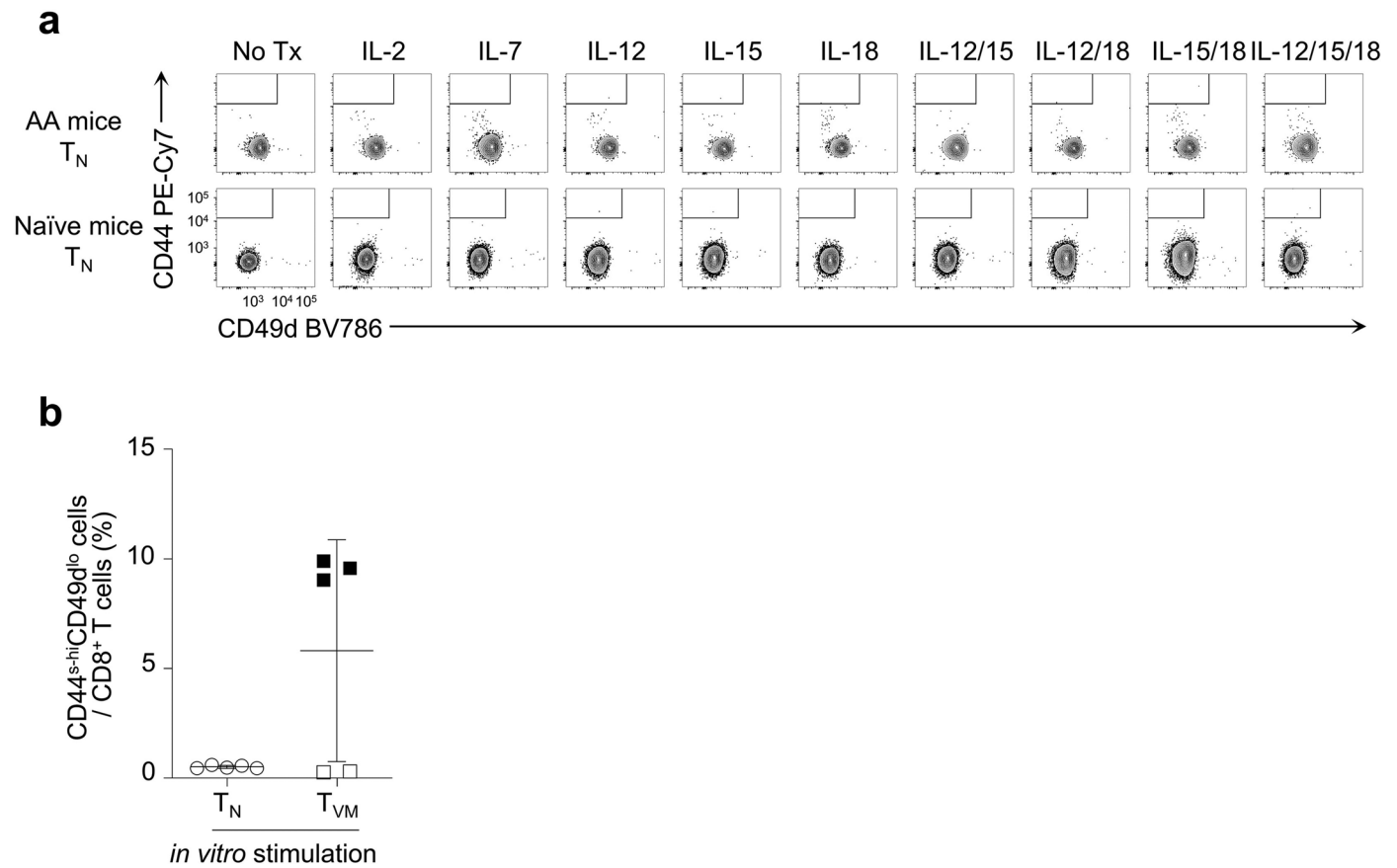
**Extended Data Fig. 4 | Conventional memory CD8<sup>+</sup> T cells primed by skin infection do not contribute to the induction of CD44<sup>hi</sup>CD49d<sup>lo</sup> CD8<sup>+</sup> T cells.** **a**, Experimental scheme for testing whether skin infection could contribute to the induction of AA. After 4 weeks of vaccinia virus (VV) infection by skin scarification, VV-infected mice (VV-AT) or naïve mice (Control-AT) were induced AA by adoptive transfer method. **b, c**, Representative flow cytometry plots (**b**) and the proportion of true memory (T<sub>TM</sub>) T cells in CD8<sup>+</sup> T cells 7 days post-VV infection ( $n = 3$ ) (**c**). **d**, Disease free ratio between the VV-AT ( $n = 8$ ), the control-

AT ( $n = 10$ ), and the historical control group ( $n = 74$ ). **e**, Representative flow cytometry plots of CD8<sup>+</sup> T cells after 12 weeks of adoptive transfer. **f**, Frequency of each cell populations in CD8<sup>+</sup> T cells ( $n = 7$ , Control-AT;  $n = 5$ , VV-AT). **g**, gMFI of the NKG2D level in each cell population ( $n = 7$ , Control-AT;  $n = 5$ , VV-AT). Data are presented as mean values  $\pm$  SD. A Log-rank (Mantel-Cox) test was used for comparison of survival curves. A Mann-Whitney test was performed for comparisons between two groups. All tests were two sided.



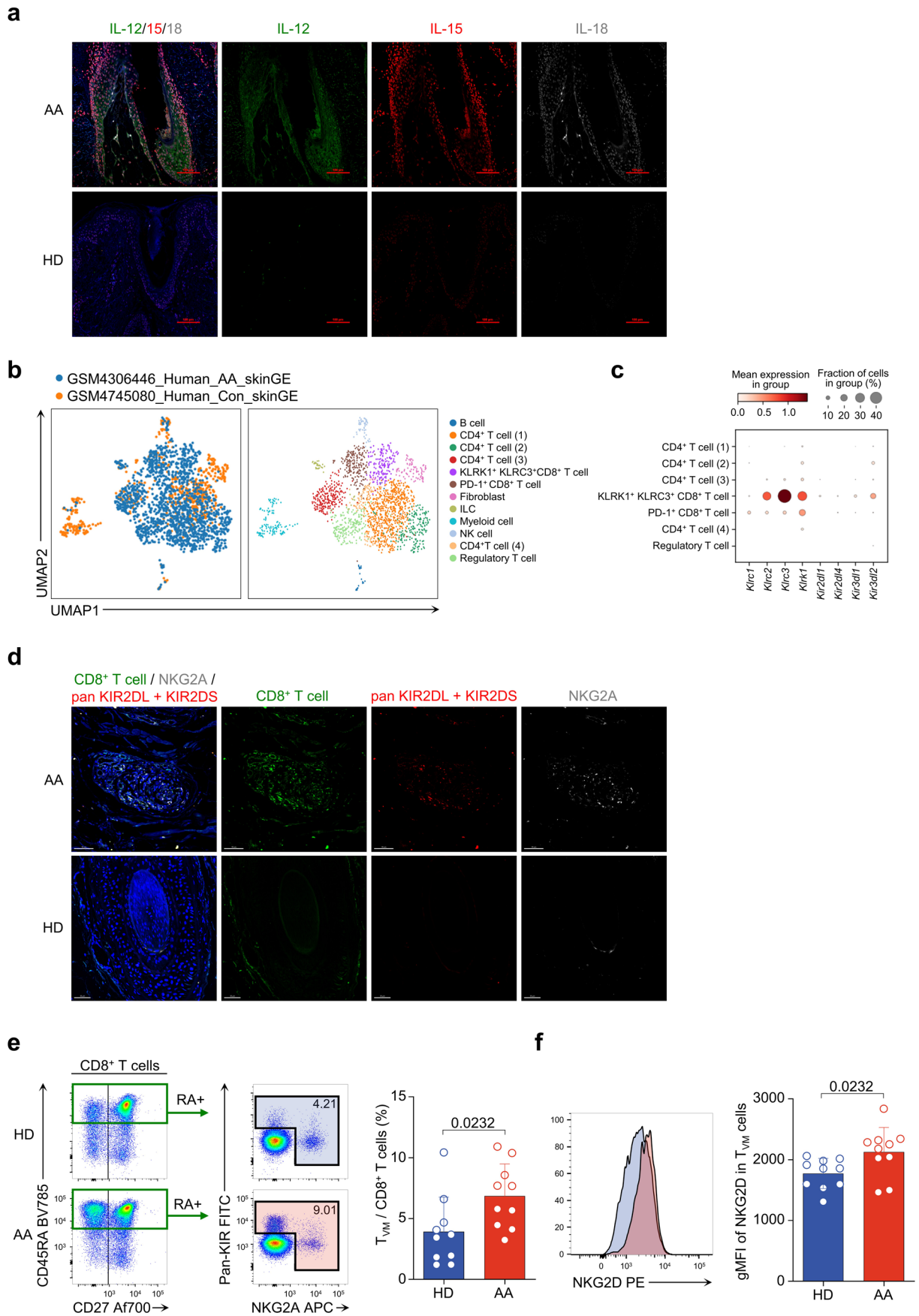
**Extended Data Fig. 5 | CD44<sup>hi</sup>CD49<sup>lo</sup>CD8<sup>+</sup> T cells are not generated by antigen-driven expansions.** **a**, Experimental scheme for evaluating the proportion of CD44<sup>hi</sup>CD49<sup>lo</sup>CD8<sup>+</sup>T cells during the AA induction process in vitro (6 days) and in vivo (> 6 weeks). **b**, The expressions of *Nr4a1*, *Nr4a2* and *Nr4a3*, which are upregulated by TCR signalling, in the SDLNs of adoptively

transferred C3H mice, measured by real-time PCR at 4 weeks after AT (before AA induction) and at a time-point post-AA onset ( $n = 4$ , naïve control;  $n = 3$ , naïve +  $\alpha$ -CD3;  $n = 5$  ( $n = 4$  in *Nr4a2*), W4;  $n = 7$ , Post-AA). Data are presented as mean values  $\pm$  SD.



**Extended Data Fig. 6 | CD44<sup>hi</sup>CD49d<sup>lo</sup> CD8<sup>+</sup> T cells originate from  $T_{VM}$  cells, not  $T_N$  cells. **a**, Representative flow cytometry plots of *in vitro*  $T_N$  cell stimulation with various cytokines. **b**, Flow cytometric analysis of SDLNs from cultured naïve**

$T_N$  and  $T_{VM}$  cell-adopted mice ( $n = 5$  mice per group). The proportion of CD44<sup>hi</sup>CD49d<sup>lo</sup> cells in CD8<sup>+</sup> T cells (closed square = AA developed mouse). Data are presented as mean values  $\pm$  SD.

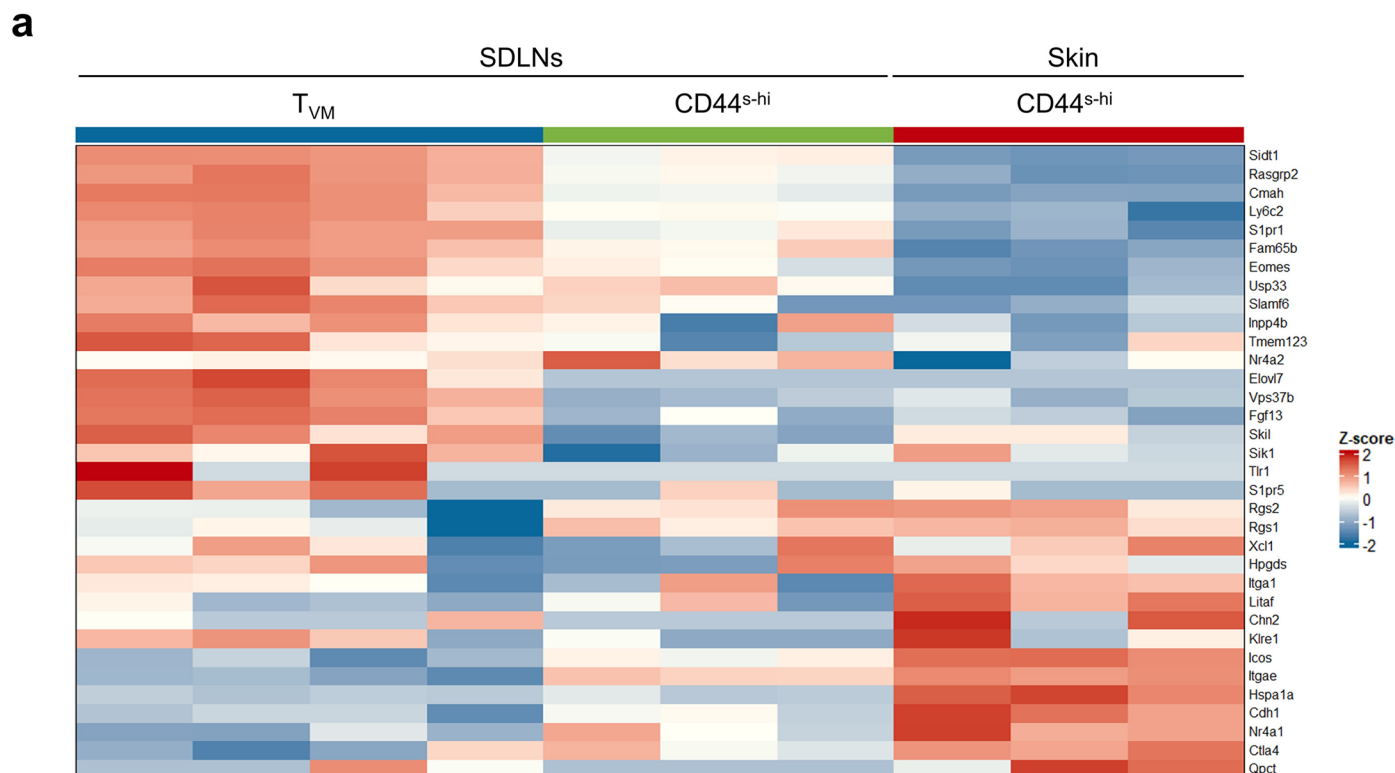


Extended Data Fig. 7 | See next page for caption.

**Extended Data Fig. 7 | T<sub>VM</sub> cells may play a crucial role in human AA pathogenesis.** **a**, IL-12, IL-15, and IL-18 staining of hair follicles from a healthy volunteer and AA patient ( $n = 3$  independent samples). Scale bars, 100  $\mu\text{m}$ . **b**, UMAP visualization of CD45<sup>+</sup> cell clusters detected in skin from AA patients and healthy volunteers. **c**, Different CD3<sup>+</sup> T-cell clusters and their gene expression levels, with brightness indicating average expression and circle size indicating the percent expression. **d**, CD8, pan-KIR2DL + KIR2DS, and NKG2A staining

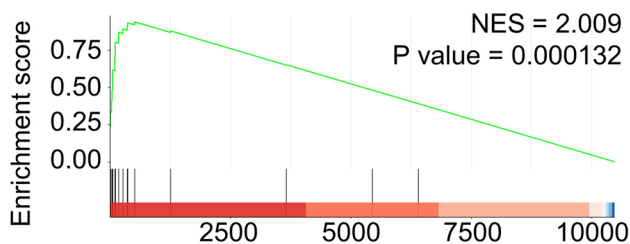
of hair follicles from a healthy volunteer and AA patient ( $n = 3$  independent samples). Scale bars, 50  $\mu\text{m}$ . **e**, **f**, PBMC CD8<sup>+</sup> T cells from healthy donors ( $n = 10$ ) and patients with AA ( $n = 10$ ) were analyzed by flow cytometry. The percentage of CD45RA<sup>+</sup>KIR<sup>+</sup>NKG2A<sup>+</sup> cells among CD8<sup>+</sup> T cells (**e**) and expression level of NKG2D in T<sub>VM</sub> cells (**f**). Data are presented as mean values  $\pm$  SD. Between-group comparisons were made using the Mann-Whitney test. All tests were two sided.



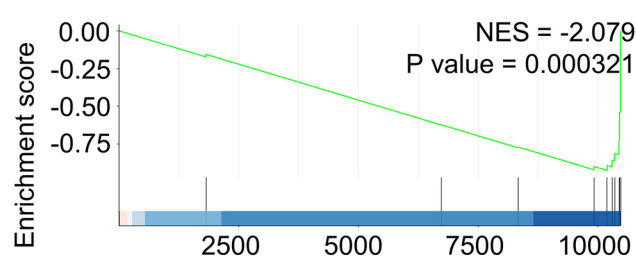


**b**  $T_{RM}$  gene set

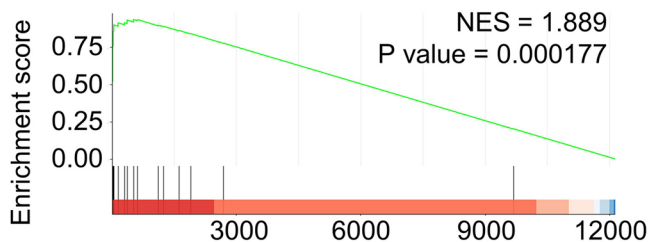
Upregulated (skin  $CD44^{s-hi}$  vs. SDLNs  $CD44^{s-hi}$ )



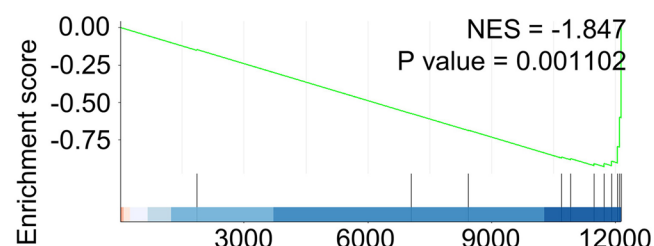
Downregulated (skin  $CD44^{s-hi}$  vs. SDLNs  $CD44^{s-hi}$ )



Upregulated (skin  $CD44^{s-hi}$  vs. SDLNs  $T_{VM}$ )

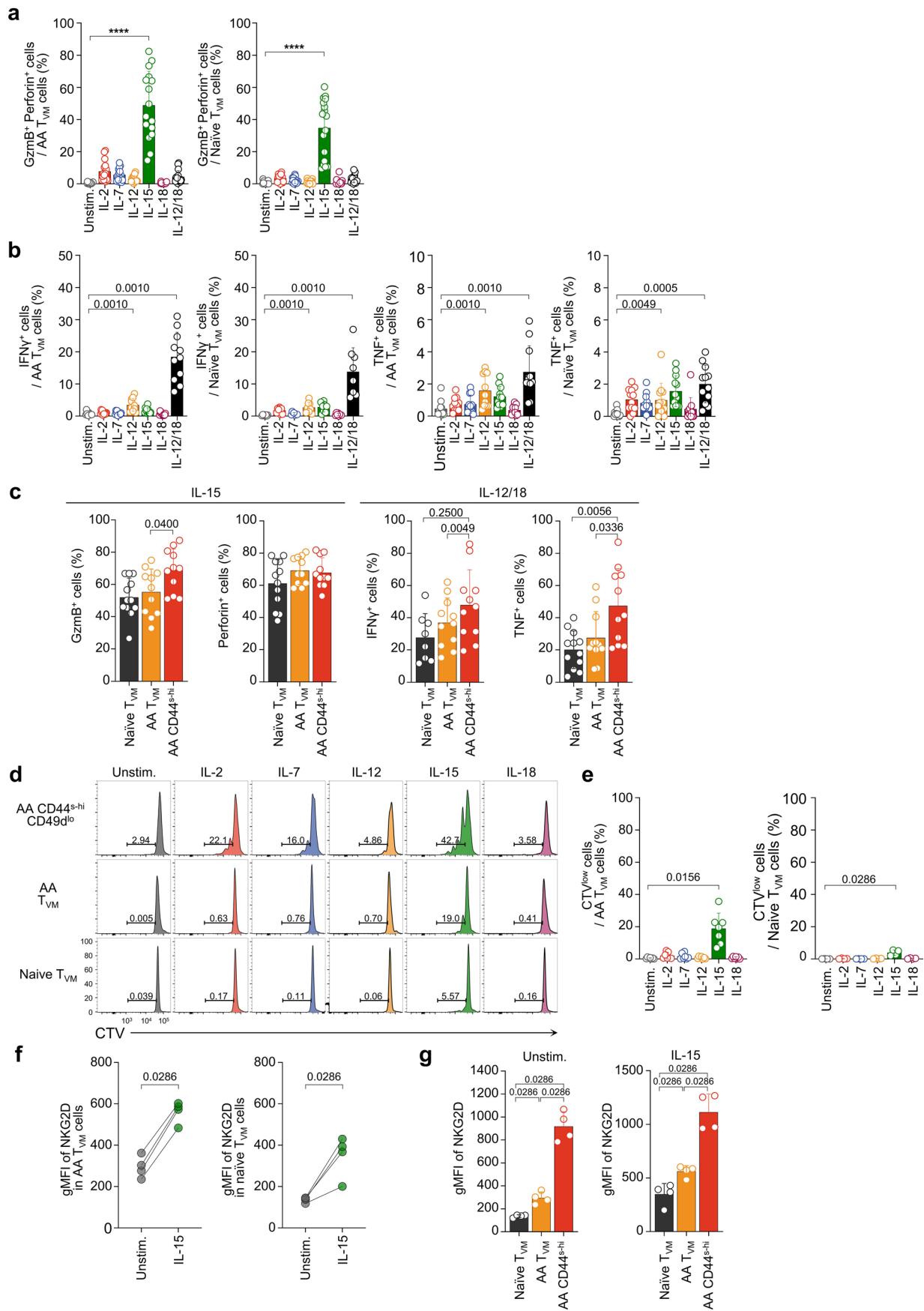


Downregulated (skin  $CD44^{s-hi}$  vs. SDLNs  $T_{VM}$ )



**Extended Data Fig. 8 |  $CD44^{s-hi}CD49d^{lo}CD8^+$  T cells from skin exhibited residential features.** **a**, Heatmap of the gene expression according to the  $T_{RM}$  gene set<sup>24</sup>. **b**, GSEA confirmed that skin  $CD44^{s-hi}CD49d^{lo}CD8^+$  T cells exhibited significant enrichment of the  $T_{RM}$  gene set<sup>24</sup> compared to  $CD44^{s-hi}CD49d^{lo}CD8^+$

T cells and  $T_{VM}$  cells from SDLNs. GSEA was performed for pairwise comparison between two groups. All tests were two sided. Data were acquired from AtAA mice. NES, normalized enrichment score.



Extended Data Fig. 9 | See next page for caption.

**Extended Data Fig. 9 | CD44<sup>hi</sup>CD49d<sup>lo</sup>CD8<sup>+</sup>T cells exhibit activation in a TCR-independent manner and enhanced proliferation capacity compared to other cell populations. a-c.** Following cytokine stimulation, various cells from SDLNs were incubated for 48 h and flow cytometric analysis performed (50 ng/ml IL-2, 50 ng/ml IL-7, 50 ng/ml IL-12, 50 ng/ml IL-15, or 50 ng/ml IL-18). **a**, The percentage of Gzmb<sup>+</sup> and perforin<sup>+</sup> cells in AA and naïve T<sub>VM</sub> cells, respectively ( $n = 16$ , AA T<sub>VM</sub>;  $n = 17$ , naïve T<sub>VM</sub>). **b**, The percentage of IFN $\gamma$ <sup>+</sup> cells ( $n = 11$ , AA T<sub>VM</sub>;  $n = 8$ , naïve T<sub>VM</sub>) and TNF<sup>+</sup> cells in AA T<sub>VM</sub> cells and naïve T<sub>VM</sub> cells ( $n = 11$ , AA T<sub>VM</sub>;  $n = 12$ , naïve T<sub>VM</sub>). **c**, Comparison of the percentage of Gzmb<sup>+</sup> cells, perforin<sup>+</sup> cells, IFN $\gamma$ <sup>+</sup> cells, and TNF<sup>+</sup> cells among each cell population in the

presence of IL-15 ( $n = 12$ , naïve;  $n = 11$ , AA) or IL-12/18 ( $n = 8$ , naïve T<sub>VM</sub>IFN $\gamma$ <sup>+</sup>;  $n = 12$ , naïve T<sub>VM</sub>TNF<sup>+</sup>;  $n = 11$ , AA). **d, e**, Following cytokine stimulation, various cells from SDLNs were incubated for 96 h. Representative flow cytometry plot of CTV<sup>low</sup> cells (**d**) and the percentage of CTV<sup>low</sup> cells in AA T<sub>VM</sub> cells ( $n = 7$ ) and naïve T<sub>VM</sub> cells ( $n = 4$ ) (**e**). **f**, gMFI of NKG2D in each cell population ( $n = 4$ , AA T<sub>VM</sub>;  $n = 4$ , naïve T<sub>VM</sub>). **g**, Comparison of the gMFI of NKG2D among each cell population without stimulation or in the presence of IL-15 ( $n = 4$  per group). Data were acquired from AtAA mice. Data are presented as mean values  $\pm$  SD. A Mann-Whitney test was performed for comparisons between two groups. All tests were two sided. \*\*\*\* $P < 0.0001$ .

## Reporting Summary

Nature Portfolio wishes to improve the reproducibility of the work that we publish. This form provides structure for consistency and transparency in reporting. For further information on Nature Portfolio policies, see our [Editorial Policies](#) and the [Editorial Policy Checklist](#).

### Statistics

For all statistical analyses, confirm that the following items are present in the figure legend, table legend, main text, or Methods section.

n/a Confirmed

- The exact sample size ( $n$ ) for each experimental group/condition, given as a discrete number and unit of measurement
- A statement on whether measurements were taken from distinct samples or whether the same sample was measured repeatedly
- The statistical test(s) used AND whether they are one- or two-sided  
*Only common tests should be described solely by name; describe more complex techniques in the Methods section.*
- A description of all covariates tested
- A description of any assumptions or corrections, such as tests of normality and adjustment for multiple comparisons
- A full description of the statistical parameters including central tendency (e.g. means) or other basic estimates (e.g. regression coefficient) AND variation (e.g. standard deviation) or associated estimates of uncertainty (e.g. confidence intervals)
- For null hypothesis testing, the test statistic (e.g.  $F$ ,  $t$ ,  $r$ ) with confidence intervals, effect sizes, degrees of freedom and  $P$  value noted  
*Give  $P$  values as exact values whenever suitable.*
- For Bayesian analysis, information on the choice of priors and Markov chain Monte Carlo settings
- For hierarchical and complex designs, identification of the appropriate level for tests and full reporting of outcomes
- Estimates of effect sizes (e.g. Cohen's  $d$ , Pearson's  $r$ ), indicating how they were calculated

*Our web collection on [statistics for biologists](#) contains articles on many of the points above.*

### Software and code

Policy information about [availability of computer code](#)

Data collection FACS LSR II (BD), FACS Aria II cell sorter (BD), MiSeq system (Illumina), HiSeqXten (Illumina), Panoramic MIDI (3DHISTECH), HD25 Nikon Confocal Microscope (Nikon), CFX-96 thermocycler (Bio-Rad), ELRO8 Elispot reader (AID), Epoch Microplate Spectrophotometer (BioTek)

Data analysis FlowJo™v.10.7.1 software for Windows  
R v.4.1.1  
Python v.3.8.5  
GraphPad Prism software v.8.0  
immunArch R package version 0.6.5  
iRweb (iRepertoire, Inc. AL, USA)  
Cell Ranger v3.1.0 (10X Genomics)  
Scanpy v1.6.1 package in Python  
Seurat package v4.0.2 in R  
Scrublet v0.2.3 package in Python  
Harmony v0.0.5 in Python  
STAR (v2.5.1b) aligner  
Weighted nearest neighbor analysis (WNN) of Seurat v4.0.2 in R  
IMARIS viewer v9.9.1  
NetMHC 4.0  
ELISpot reader v7.0(AID)  
Case Viewer software v2.2  
BioTek Gen5 Software for Imaging & Microscopy v5.10

```
Bio-Rad CFX Manager 2.0 FILE V.2.0.885.0923
BIOCARTA_TCR_PATHWAY : https://www.gsea-msigdb.org/gsea/msigdb/cards/BIOCARTA_TCR_PATHWAY
TRM gene set : GSE47045
GOLDRATH_EFF_VS_MEMORY_CD8_T CELL : GSE1000002_1582_200_UP, SE1000002_1582_200_DN
```

For manuscripts utilizing custom algorithms or software that are central to the research but not yet described in published literature, software must be made available to editors and reviewers. We strongly encourage code deposition in a community repository (e.g. GitHub). See the Nature Portfolio [guidelines for submitting code & software](#) for further information.

## Data

Policy information about [availability of data](#)

All manuscripts must include a [data availability statement](#). This statement should provide the following information, where applicable:

- Accession codes, unique identifiers, or web links for publicly available datasets
- A description of any restrictions on data availability
- For clinical datasets or third party data, please ensure that the statement adheres to our [policy](#)

The single cell RNA-sequencing data and bulk RNA-sequencing data has been deposited in the GEO database under the primary accession codes GSE229631. The sequences were aligned to the mm10 mouse reference genome from UCSC. TCR sequencing data is provided as a separate 'Supplementary data file'. The data that support the findings of this study are available from the corresponding author upon request.

## Human research participants

Policy information about [studies involving human research participants and Sex and Gender in Research](#).

Reporting on sex and gender

This study is not limited to a singular sex. 10 healthy donors (6 males and 4 females) and 10 patients with alopecia areata (5 males and 5 females) were enrolled in the study.

Population characteristics

For this study, we enrolled 10 AA patients with 3 months of treatment cessation, and 10 healthy volunteers. Detailed clinical information of the enrolled AA patients including age, gender, race, SALT score, duration of disease, and comorbidity is provided in Supplementary Table 4.

Recruitment

10 healthy volunteers and 10 AA patients were enrolled by a public announcement for recruitment, for whom they received a routine health checkup or suffered from alopecia areata, respectively. No self-selection biases or other biases are present in the subjects' enrollment.

Ethics oversight

This study was reviewed and approved by the institutional review boards (IRB) of Chung-Ang University Hospital (IRB approval number : CAU-DERMA-AA01) and conducted in accordance with the principles of the Declaration of Helsinki. Informed consent was obtained from all participants. All participants received financial compensation.

Note that full information on the approval of the study protocol must also be provided in the manuscript.

## Field-specific reporting

Please select the one below that is the best fit for your research. If you are not sure, read the appropriate sections before making your selection.

- Life sciences       Behavioural & social sciences       Ecological, evolutionary & environmental sciences

For a reference copy of the document with all sections, see [nature.com/documents/nr-reporting-summary-flat.pdf](https://www.nature.com/documents/nr-reporting-summary-flat.pdf)

## Life sciences study design

All studies must disclose on these points even when the disclosure is negative.

Sample size

Mouse sample sizes was described in the legends of each figure. No statistical methods were used to pre-determine sample sizes but our sample sizes are similar to those reported in previous publications.

Data exclusions

No data points or mice were excluded for analysis in this study.

Replication

3 independent repeats were performed for each experiment with independent sets of mice for in vivo experiments. The experimental findings were reliably reproduced.

Randomization

Age-matched mice were randomly allocated.

Blinding

Data collection and analysis were not performed blind to the conditions of the experiments.

## Behavioural & social sciences study design

All studies must disclose on these points even when the disclosure is negative.

Study description	Briefly describe the study type including whether data are quantitative, qualitative, or mixed-methods (e.g. qualitative cross-sectional, quantitative experimental, mixed-methods case study).
Research sample	State the research sample (e.g. Harvard university undergraduates, villagers in rural India) and provide relevant demographic information (e.g. age, sex) and indicate whether the sample is representative. Provide a rationale for the study sample chosen. For studies involving existing datasets, please describe the dataset and source.
Sampling strategy	Describe the sampling procedure (e.g. random, snowball, stratified, convenience). Describe the statistical methods that were used to predetermine sample size OR if no sample-size calculation was performed, describe how sample sizes were chosen and provide a rationale for why these sample sizes are sufficient. For qualitative data, please indicate whether data saturation was considered, and what criteria were used to decide that no further sampling was needed.
Data collection	Provide details about the data collection procedure, including the instruments or devices used to record the data (e.g. pen and paper, computer, eye tracker, video or audio equipment) whether anyone was present besides the participant(s) and the researcher, and whether the researcher was blind to experimental condition and/or the study hypothesis during data collection.
Timing	Indicate the start and stop dates of data collection. If there is a gap between collection periods, state the dates for each sample cohort.
Data exclusions	If no data were excluded from the analyses, state so OR if data were excluded, provide the exact number of exclusions and the rationale behind them, indicating whether exclusion criteria were pre-established.
Non-participation	State how many participants dropped out/declined participation and the reason(s) given OR provide response rate OR state that no participants dropped out/declined participation.
Randomization	If participants were not allocated into experimental groups, state so OR describe how participants were allocated to groups, and if allocation was not random, describe how covariates were controlled.

## Ecological, evolutionary & environmental sciences study design

All studies must disclose on these points even when the disclosure is negative.

Study description	Briefly describe the study. For quantitative data include treatment factors and interactions, design structure (e.g. factorial, nested, hierarchical), nature and number of experimental units and replicates.
Research sample	Describe the research sample (e.g. a group of tagged <i>Passer domesticus</i> , all <i>Stenocereus thurberi</i> within Organ Pipe Cactus National Monument), and provide a rationale for the sample choice. When relevant, describe the organism taxa, source, sex, age range and any manipulations. State what population the sample is meant to represent when applicable. For studies involving existing datasets, describe the data and its source.
Sampling strategy	Note the sampling procedure. Describe the statistical methods that were used to predetermine sample size OR if no sample-size calculation was performed, describe how sample sizes were chosen and provide a rationale for why these sample sizes are sufficient.
Data collection	Describe the data collection procedure, including who recorded the data and how.
Timing and spatial scale	Indicate the start and stop dates of data collection, noting the frequency and periodicity of sampling and providing a rationale for these choices. If there is a gap between collection periods, state the dates for each sample cohort. Specify the spatial scale from which the data are taken
Data exclusions	If no data were excluded from the analyses, state so OR if data were excluded, describe the exclusions and the rationale behind them, indicating whether exclusion criteria were pre-established.
Reproducibility	Describe the measures taken to verify the reproducibility of experimental findings. For each experiment, note whether any attempts to repeat the experiment failed OR state that all attempts to repeat the experiment were successful.
Randomization	Describe how samples/organisms/participants were allocated into groups. If allocation was not random, describe how covariates were controlled. If this is not relevant to your study, explain why.
Blinding	Describe the extent of blinding used during data acquisition and analysis. If blinding was not possible, describe why OR explain why blinding was not relevant to your study.

Did the study involve field work?  Yes  No

## Field work, collection and transport

Field conditions	<i>Describe the study conditions for field work, providing relevant parameters (e.g. temperature, rainfall).</i>
Location	<i>State the location of the sampling or experiment, providing relevant parameters (e.g. latitude and longitude, elevation, water depth).</i>
Access & import/export	<i>Describe the efforts you have made to access habitats and to collect and import/export your samples in a responsible manner and in compliance with local, national and international laws, noting any permits that were obtained (give the name of the issuing authority, the date of issue, and any identifying information).</i>
Disturbance	<i>Describe any disturbance caused by the study and how it was minimized.</i>

## Reporting for specific materials, systems and methods

We require information from authors about some types of materials, experimental systems and methods used in many studies. Here, indicate whether each material, system or method listed is relevant to your study. If you are not sure if a list item applies to your research, read the appropriate section before selecting a response.

### Materials & experimental systems

n/a	Involved in the study
<input type="checkbox"/>	<input checked="" type="checkbox"/> Antibodies
<input type="checkbox"/>	<input checked="" type="checkbox"/> Eukaryotic cell lines
<input checked="" type="checkbox"/>	<input type="checkbox"/> Palaeontology and archaeology
<input type="checkbox"/>	<input checked="" type="checkbox"/> Animals and other organisms
<input checked="" type="checkbox"/>	<input type="checkbox"/> Clinical data
<input checked="" type="checkbox"/>	<input type="checkbox"/> Dual use research of concern

### Methods

n/a	Involved in the study
<input checked="" type="checkbox"/>	<input type="checkbox"/> ChIP-seq
<input type="checkbox"/>	<input checked="" type="checkbox"/> Flow cytometry
<input checked="" type="checkbox"/>	<input type="checkbox"/> MRI-based neuroimaging

## Antibodies

### Antibodies used

<Flow cytometry>  
 -Mouse  
 Brilliant Violet 510™ anti-mouse CD3 Antibody: 17A2; Biolegend; 100234; Lot: B335589, (dilution factor 1:200)  
 BV421 Rat Anti-Mouse CD8a: 53-6.7; BD Bioscience; 563898; Lot: 0310529, (dilution factor 1:200)  
 PerCP-Cy™5.5 Rat Anti-Mouse CD8a: 53-6.7; BD Bioscience; 561109; Lot: 9098816, (dilution factor 1:200)  
 APC-Cy™7 Rat Anti-Mouse CD8a: 53-6.7; BD Bioscience; 557654; Lot: 1005004, (dilution factor 1:200)  
 BV421 Rat Anti-Mouse CD44: IM7; BD Bioscience; 563970; Lot: 1228934, (dilution factor 1:200)  
 PE-Cy™7 Rat Anti-Mouse CD44: IM7; BD Bioscience; 560569; Lot: 9102731, (dilution factor 1:200)  
 Alexa Fluor® 700 Rat Anti-Mouse CD44: IM7; BD Bioscience; 560567; Lot: 9121530, (dilution factor 1:200)  
 APC-Cy™7 Rat Anti-Mouse CD44: IM7; BD Bioscience; 560568; Lot: 1083068, (dilution factor 1:200)  
 PE/Cyanine7 anti-mouse CD49d: R1-2; Biolegend; 103618; Lot: B316078, (dilution factor 1:200)  
 BV786 Rat Anti-Mouse CD49d: R1-2; BD Bioscience; 564397; Lot: 1011266, (dilution factor 1:200)  
 BV650 Rat Anti-Mouse CD62L: MEL-14; BD Bioscience; 564108; Lot: 1239350, (dilution factor 1:200)  
 APC anti-mouse CD314 (NKG2D): CX5; Biolegend; 130212; Lot: B281111, (dilution factor 1:100)  
 FITC anti-human/mouse Granzyme B: QA16A02; Biolegend; 372206; Lot: B274306, (dilution factor 1:100)  
 PE anti-mouse Perforin Antibody: S16009A; Biolegend; 154306; Lot: B295837, (dilution factor 1:100)  
 BV711 Rat Anti-Mouse IFN-γ: XMG1.2; BD Bioscience; 564336; Lot: 1032459, (dilution factor 1:100)  
 PE-Cy™7 Rat Anti-Mouse TNF: MP6-XT22; BD Bioscience, 557644; Lot: 0155357, (dilution factor 1:100)  
 Alexa Fluor® 700 Mouse anti-Ki-67: B56; BD Bioscience, 561277; Lot: 9315354, (dilution factor 1:100)  
 BV786 Mouse Anti-Ki-67: B56; BD Bioscience, 563756; Lot: 9267698, (dilution factor 1:100)  
 PE anti-mouse Nur77: 12.14; eBioscience™; 12-5965-82; Lot: 2055181, (dilution factor 1:100)  
 PE Rat Anti-Mouse CD103: M290; BD Bioscience; 557495; Lot: 7264512, (dilution factor 1:200)  
 PerCP/Cyanine5.5 anti-mouse CD49a : HMα1; Biolegend; 142612; Lot: 1243769, (dilution factor 1:200)  
 Alexa Fluor® 700 Rat Anti-Mouse TCR β chain Antibody: H57-597; Biolegend; 560567; Lot: 9121530, (dilution factor 1:200)  
 FITC Hamster Anti-Mouse γδ T-Cell Receptor : GL3; BD Bioscience; 109224; Lot: B308382, (dilution factor 1:200)  
 PE-CF594 Rat Anti-Mouse CD19: 1D3; BD Bioscience; 562291; Lot: 1243026, (dilution factor 1:200)  
 PE-CF594 Rat Anti-Mouse CD14 : rmC5-3; BD Bioscience; 564145; Lot: 2124921, (dilution factor 1:200)  
 PE-conjugated Dextramer (IEGGWTGMI): Immudex (dilution factor 1:20)  
  
 -Human, (dilution 1:50)  
 BV711 Mouse Anti-Human CD3: UCHT-1; BD Bioscience; 563724; Lot: 1098392, (dilution factor 1:100)  
 APC-Cy™7 Mouse Anti-Human CD8: SK1; BD Bioscience; 561945; Lot: 9031898, (dilution factor 1:100)  
 BV650 Mouse Anti-Human CD161: DX12; BD Bioscience; 563864; Lot: 1117428, (dilution factor 1:100)  
 Brilliant Violet 785™ anti-human CD45RA: HI100; Biolegend; 304140; Lot: 1083671, (dilution factor 1:100)  
 Alexa Fluor® 700 Mouse Anti-Human CD27: M-T271; BD Bioscience; 560611; Lot: 1050268, (dilution factor 1:100)

FITC anti-human KIR2D, REAfinity™: REA1042; Miltenyi Biotec; 130-117-477; Lot: 5210401043, (dilution factor 1:50)  
 CD158e/k (KIR3DL1/DL2) Antibody, anti-human, REAfinity™ : REA970; Miltenyi Biotec; 130-116-177; Lot: 5210401104, (dilution factor 1:50)  
 CD159a (NKG2A) Antibody, anti-human, REAfinity™ : REA110; Miltenyi Biotec; 130-114-089; Lot: 5210201607, (dilution factor 1:50)  
 PE anti-human CD314 (NKG2D) Antibody : 1D11; Biolegend; 320806; Lot: B266061, (dilution factor 1:100)

<Immunofluorescence analysis>

-Mouse

anti-IL12 (Invitrogen, 9A5, MM120) (dilution factor 1:100), anti-IL15 (R&D systems, polyclonal, AF447) (dilution factor 1:500), anti-IL18 (Abcam, EPR22249-212, ab223293) (dilution factor 1:100), anti-CD45 (R&D systems, polyclonal, AF114) (dilution factor 1:100), anti-CK14 (Abcam, ERP17350, ab181595) (dilution factor 1:100)

-Human

anti-IL12 (Abcam, polyclonal, ab124635) (dilution factor 1:100), anti-IL15 (Abcam, 3A3, ab55276) (dilution factor 1:150), anti-IL18 (Abcam, polyclonal, ab191152) (dilution factor 1:250), anti-CD8 (dilution factor Bio-rad, YTC182.20, MCA351G) (1:100), anti-NKG2A (R&D Systems, 131411, MAB1059-100) (dilution factor 1:100), anti-KIR2DL (Abcam, EPR22492-64, ab255327) (dilution factor 1:200)

-2nd antibody

Alexa Fluor® 488 AffiniPure Donkey Anti-Rabbit IgG (H+L) : Jackson ImmunoResearch; 711-545-152; RRID: AB\_2313584 (dilution factor 1:400)

Alexa Fluor® 594 AffiniPure Donkey Anti-Rabbit IgG (H+L) : Jackson ImmunoResearch; 711-585-152; RRID: AB\_2340621 (dilution factor 1:400)

Alexa Fluor® 647 AffiniPure Donkey Anti-Rabbit IgG (H+L) : Jackson ImmunoResearch; 711-605-152; RRID: AB\_2492288 (dilution factor 1:400)

Alexa Fluor® 488 AffiniPure Donkey Anti-Goat IgG (H+L) : Jackson ImmunoResearch; 705-545-003; RRID: AB\_2340428 (dilution factor 1:400)

Alexa Fluor® 594 AffiniPure Donkey Anti-Goat IgG (H+L) : Jackson ImmunoResearch; 705-585-003; RRID: AB\_2340432 (dilution factor 1:400)

Alexa Fluor® 647 AffiniPure Donkey Anti-Goat IgG (H+L) : Jackson ImmunoResearch; 705-605-003; RRID: AB\_2340436 (dilution factor 1:400)

Alexa Fluor® 488 AffiniPure Donkey Anti-Rat IgG (H+L) : Jackson ImmunoResearch; 712-545-150; RRID: AB\_2340683 (dilution factor 1:400)

Alexa Fluor® 594 AffiniPure Donkey Anti-Rat IgG (H+L) : Jackson ImmunoResearch; 712-585-150; RRID: AB\_2340688 (dilution factor 1:400)

Alexa Fluor® 594 AffiniPure Donkey Anti-Mouse IgG (H+L) : Jackson ImmunoResearch; 715-585-150; RRID: AB\_2340854 (dilution factor 1:400)

Alexa Fluor® 647 AffiniPure Donkey Anti-Mouse IgG (H+L) : Jackson ImmunoResearch; 715-605-150; RRID: AB\_2340862 (dilution factor 1:400)

## Validation

-Mouse

Brilliant Violet 510™ anti-mouse CD3 Antibody : <https://www.biolegend.com/en-us/products/brilliant-violet-510-anti-mouse-cd3-antibody-7990>

BV421 Rat Anti-Mouse CD8a : <https://www.bdbiosciences.com/ko-kr/products/reagents/flow-cytometry-reagents/research-reagents/single-color-antibodies-ruo/bv421-rat-anti-mouse-cd8a.563898>

PerCP-Cy™5.5 Rat Anti-Mouse CD8a : <https://www.bdbiosciences.com/ko-kr/products/reagents/flow-cytometry-reagents/research-reagents/single-color-antibodies-ruo/percp-cy-5-5-rat-anti-mouse-cd8a.561109>

APC-Cy™7 Rat Anti-Mouse CD8a : <https://www.bdbiosciences.com/ko-kr/products/reagents/flow-cytometry-reagents/research-reagents/single-color-antibodies-ruo/apc-cy-7-rat-anti-mouse-cd8a.557654>

BV421 Rat Anti-Mouse CD44 : <https://www.bdbiosciences.com/ko-kr/products/reagents/flow-cytometry-reagents/research-reagents/single-color-antibodies-ruo/bv421-rat-anti-mouse-cd44.563970>

PE-Cy™7 Rat Anti-Mouse CD44 : <https://www.bdbiosciences.com/en-us/products/reagents/flow-cytometry-reagents/research-reagents/single-color-antibodies-ruo/pe-cy-7-rat-anti-mouse->

Alexa Fluor® 700 Rat Anti-Mouse CD44 : <https://www.bdbiosciences.com/en-us/products/reagents/flow-cytometry-reagents/research-reagents/single-color-antibodies-ruo/alexa-fluor-700-rat-anti-mouse-cd44.560567>

APC-Cy™7 Rat Anti-Mouse CD44 : <https://www.bdbiosciences.com/ko-kr/products/reagents/flow-cytometry-reagents/research-reagents/single-color-antibodies-ruo/apc-cy-7-rat-anti-mouse-cd44.560568>

PE/Cyanine7 anti-mouse CD49d Antibody : <https://www.biolegend.com/en-us/products/pe-cyanine7-anti-mouse-cd49d-antibody-9900>

BV786 Rat Anti-Mouse CD49d : <https://www.bdbiosciences.com/ko-kr/products/reagents/flow-cytometry-reagents/research-reagents/single-color-antibodies-ruo/bv786-rat-anti-mouse-cd49d.564397>

BV650 Rat Anti-Mouse CD62L : <https://www.bdbiosciences.com/ko-kr/products/reagents/flow-cytometry-reagents/research-reagents/single-color-antibodies-ruo/bv650-rat-anti-mouse-cd62l.564108>

APC anti-mouse CD314 (NKG2D) Antibody : <https://www.biolegend.com/en-us/products/apc-anti-mouse-cd314-nkg2d-antibody-5267?GroupID=BLG10492>

FITC anti-human/mouse Granzyme B Recombinant Antibody : <https://www.biolegend.com/en-us/products/fitc-anti-human-mouse-granzyme-b-recombinant-antibody-14430?GroupID=GROUP28>

PE anti-mouse Perforin Antibody : <https://www.biolegend.com/en-us/products/pe-anti-mouse-perforin-antibody-15255?GroupID=GROUP20>

BV711 Rat Anti-Mouse IFN-γ : <https://www.bdbiosciences.com/zh-cn/products/reagents/flow-cytometry-reagents/research-reagents/single-color-antibodies-ruo/bv711-rat-anti-mouse-ifn.564336>

PerCP-Cy™5.5 Rat Anti-Mouse TNF : <https://www.bdbiosciences.com/en-tw/products/reagents/flow-cytometry-reagents/research-reagents/single-color-antibodies-ruo/percp-cy-5-5-rat-anti-mouse-tnf.560659>

Alexa Fluor® 700 Mouse anti-Ki-67 : <https://www.bdbiosciences.com/ko-kr/products/reagents/flow-cytometry-reagents/research-reagents/single-color-antibodies-ruo/alexa-fluor-700-mouse-anti-ki-67.561277>

BV786 Mouse Anti-Ki-67 : <https://www.bdbiosciences.com/ko-kr/products/reagents/flow-cytometry-reagents/research-reagents/single-color-antibodies-ruo/bv786-mouse-anti-ki-67.563756>

Nur77 Monoclonal Antibody (12.14), P

E, eBioscience™ : <https://www.thermofisher.com/antibody/product/Nur77-Antibody-clone-12-14-Monoclonal/12-5965-82>



PE Rat Anti-Mouse CD103 : <https://wwwbdbiosciences.com/ko-kr/products/reagents/flow-cytometry-reagents/research-reagents/single-color-antibodies-ruo/pe-rat-anti-mouse-cd103.557495>  
 PerCP/Cyanine5.5 anti-mouse CD49a Antibody : <https://www.biolegend.com/en-us/products/percp-cyanine5-5-anti-mouse-cd49a-antibody-16347?GroupID=BLG9664>  
 Alexa Fluor® 700 Rat Anti-Mouse TCR β chain Antibody : <https://www.biolegend.com/en-us/products/alexa-fluor-700-anti-mouse-tcr-beta-chain-antibody-4537>  
 FITC Hamster Anti-Mouse γδ T-Cell Receptor : <https://wwwbdbiosciences.com/ko-kr/products/reagents/flow-cytometry-reagents/research-reagents/single-color-antibodies-ruo/fitc-hamster-anti-mouse-t-cell-receptor.553177>  
 PE-CF594 Rat Anti-Mouse CD19 : <https://wwwbdbiosciences.com/ko-kr/products/reagents/flow-cytometry-reagents/research-reagents/single-color-antibodies-ruo/pe-cf594-rat-anti-mouse-cd19.562291>  
 PE-CF594 Rat Anti-Mouse CD14 : <https://wwwbdbiosciences.com/ko-kr/products/reagents/flow-cytometry-reagents/research-reagents/single-color-antibodies-ruo/pe-cf594-rat-anti-mouse-cd14.564145>  
 PE-conjugated Dextramer (IEGGWTGMI); Supplementary Fig. 1

-Human

BV711 Mouse Anti-Human CD3 : <https://wwwbdbiosciences.com/ko-kr/products/reagents/flow-cytometry-reagents/research-reagents/single-color-antibodies-ruo/bv711-mouse-anti-human-cd3.563724>  
 APC-Cy™7 Mouse Anti-Human CD8 : <https://wwwbdbiosciences.com/ko-kr/products/reagents/flow-cytometry-reagents/research-reagents/single-color-antibodies-ruo/apc-cy-7-mouse-anti-human-cd8.561945>  
 BV650 Mouse Anti-Human CD161 : <https://wwwbdbiosciences.com/ko-kr/products/reagents/flow-cytometry-reagents/research-reagents/single-color-antibodies-ruo/bv650-mouse-anti-human-cd161.563864>  
 Brilliant Violet 785™ anti-human CD45RA Antibody : <https://www.biolegend.com/en-us/products/brilliant-violet-785-anti-human-cd45ra-antibody-7972>  
 Alexa Fluor® 700 Mouse Anti-Human CD27 : <https://wwwbdbiosciences.com/ko-kr/products/reagents/flow-cytometry-reagents/research-reagents/single-color-antibodies-ruo/alexa-fluor-700-mouse-anti-human-cd27.560611>  
 KIR2D Antibody, anti-human, REAfinity™ : <https://www.miltenyibiotec.com/IS-en/products/kir2d-antibody-anti-human-reafinity-rea1042.html#gref>  
 CD158e/k (KIR3DL1/DL2) Antibody, anti-human, REAfinity™ : <https://www.miltenyibiotec.com/IS-en/products/cd158e-k-kir3dl1-dl2-antibody-anti-human-reafinity-rea970.html?countryRedirected=1#gref>  
 CD159a (NKG2A) Antibody, anti-human, REAfinity™ : <https://www.miltenyibiotec.com/IS-en/products/cd159a-nkg2a-antibody-anti-human-reafinity-rea110.html?countryRedirected=1#gref>  
 PE anti-human CD314 (NKG2D) Antibody : <https://www.biolegend.com/en-us/products/pe-anti-human-cd314-nkg2d-antibody-3016?GroupID=BLG4241>

<Immunofluorescence analysis>

-Mouse

IL-12 p70 Monoclonal Antibody (9A5) : <https://www.thermofisher.com/antibody/product/IL-12-p70-Antibody-clone-9A5-Monoclonal/MM120>  
 Mouse IL-15 Antibody : [https://www.rndsystems.com/products/mouse-il-15-antibody\\_af447](https://www.rndsystems.com/products/mouse-il-15-antibody_af447)  
 Recombinant Anti-IL-18 antibody [EPR22249-212] (ab223293) : <https://www.abcam.com/il-18-antibody-epr22249-212-ab223293.html>  
 Mouse CD45 Antibody : [https://www.rndsystems.com/products/mouse-cd45-antibody\\_af114](https://www.rndsystems.com/products/mouse-cd45-antibody_af114)  
 Recombinant Anti-Cytokeratin 14 antibody [EPR17350] - Cytoskeleton Marker (ab181595) : <https://www.abcam.com/cytokeratin-14-antibody-epr17350-cytoskeleton-marker-ab181595.html>

-Human

Anti-IL-12 antibody (ab124635) : <https://www.abcam.com/il-12-antibody-ab124635.html>  
 Anti-IL-15 antibody [3A3] (ab55276) : <https://www.abcam.com/il-15-antibody-3a3-ab55276.html>  
 Anti-IL-18 antibody (ab191152) : <https://www.abcam.com/il-18-antibody-ab191152.html>  
 CD8 antibody, YTC182.20 : [https://www.bio-rad-antibodies.com/monoclonal/human-cd8-antibody-ytic182-20-mca351.html?f=purified&JSESSIONID\\_STERLING=B6D7D2CC186A7E2153EB3CAA04B5053.ecommerce1&evCntryLang=KR-ko&cntry=KR&thirdPartyCookieEnabled=true](https://www.bio-rad-antibodies.com/monoclonal/human-cd8-antibody-ytic182-20-mca351.html?f=purified&JSESSIONID_STERLING=B6D7D2CC186A7E2153EB3CAA04B5053.ecommerce1&evCntryLang=KR-ko&cntry=KR&thirdPartyCookieEnabled=true)  
 Human NKG2A/CD159a Antibody : [https://www.rndsystems.com/products/human-nkg2a-cd159a-antibody-131411\\_mab1059](https://www.rndsystems.com/products/human-nkg2a-cd159a-antibody-131411_mab1059)  
 Recombinant Anti-KIR2DL3 + KIR2DL1 + KIR2DS2 + KIR2DL2 + KIR2DS1 antibody [EPR22492-64] - BSA and Azide free (ab255327) : <https://www.abcam.com/kir2dl3--kir2dl1--kir2ds2--kir2dl2--kir2ds1-antibody-epr22492-64-bsa-and-azide-free-ab255327.html>

-2nd antibody

Alexa Fluor® 488 AffiniPure Donkey Anti-Rabbit IgG (H+L) : <https://www.jacksonimmuno.com/catalog/products/711-545-152>  
 Alexa Fluor® 594 AffiniPure Donkey Anti-Rabbit IgG (H+L) : <https://www.jacksonimmuno.com/catalog/products/711-585-152>  
 Alexa Fluor® 647 AffiniPure Donkey Anti-Rabbit IgG (H+L) : <https://www.jacksonimmuno.com/catalog/products/711-605-152>  
 Alexa Fluor® 488 AffiniPure Donkey Anti-Goat IgG (H+L) : <https://www.jacksonimmuno.com/catalog/products/705-545-003>  
 Alexa Fluor® 594 AffiniPure Donkey Anti-Goat IgG (H+L) : <https://www.jacksonimmuno.com/catalog/products/705-585-003>  
 Alexa Fluor® 647 AffiniPure Donkey Anti-Goat IgG (H+L) : <https://www.jacksonimmuno.com/catalog/products/705-605-003>  
 Alexa Fluor® 488 AffiniPure Donkey Anti-Rat IgG (H+L) : <https://www.jacksonimmuno.com/catalog/products/712-545-150>  
 Alexa Fluor® 594 AffiniPure Donkey Anti-Rat IgG (H+L) : <https://www.jacksonimmuno.com/catalog/products/712-585-150>  
 Alexa Fluor® 594 AffiniPure Donkey Anti-Mouse IgG (H+L) : <https://www.jacksonimmuno.com/catalog/products/715-585-150>  
 Alexa Fluor® 647 AffiniPure Donkey Anti-Mouse IgG (H+L) : <https://www.jacksonimmuno.com/catalog/products/715-605-150>

## Eukaryotic cell lines

Policy information about [cell lines and Sex and Gender in Research](#)

Cell line source(s)

The YAC-1 cell line was originally obtained from ATCC.

Authentication	Certificate of analysis was provided by ATCC at the time of purchasing. Other than this, no specific authentication was performed specifically.
Mycoplasma contamination	The YAC-1 cell line has been tested for mycoplasma negative in the past years.
Commonly misidentified lines (See <a href="#">ICLAC</a> register)	The YAC-1 cell line was not among the misidentified cell lines published from the most recent version 12.0 of the database.

## Palaeontology and Archaeology

Specimen provenance	<i>Provide provenance information for specimens and describe permits that were obtained for the work (including the name of the issuing authority, the date of issue, and any identifying information). Permits should encompass collection and, where applicable, export.</i>
Specimen deposition	<i>Indicate where the specimens have been deposited to permit free access by other researchers.</i>
Dating methods	<i>If new dates are provided, describe how they were obtained (e.g. collection, storage, sample pretreatment and measurement), where they were obtained (i.e. lab name), the calibration program and the protocol for quality assurance OR state that no new dates are provided.</i>
<input type="checkbox"/>	Tick this box to confirm that the raw and calibrated dates are available in the paper or in Supplementary Information.
Ethics oversight	<i>Identify the organization(s) that approved or provided guidance on the study protocol, OR state that no ethical approval or guidance was required and explain why not.</i>

Note that full information on the approval of the study protocol must also be provided in the manuscript.

## Animals and other research organisms

Policy information about [studies involving animals](#); [ARRIVE guidelines](#) recommended for reporting animal research, and [Sex and Gender in Research](#)

Laboratory animals	Mus musculus (mouse), C3H/HeJ (Jackson Lab), Female, 8-12 weeks Mice were provided solid diet (Envigo, 2018C) throughout the experimental period, allowing them to freely consume. The mice were acclimated for one week under controlled conditions of temperature ( $23 \pm 2$ °C), humidity ( $55 \pm 10\%$ ), and a 12-hour light-dark cycle before being used for the subsequent experiments.
Wild animals	Not used
Reporting on sex	According to previous studies, induction of alopecia areata (AA) is only possible in C3H/HeJ females. Therefore, only female mice were considered as a model in this study.
Field-collected samples	Not used
Ethics oversight	All animal studies were conducted following protocols approved by Institutional Animal Care and Use Committee (IACUC) of KAIST. (KA2019-55).

Note that full information on the approval of the study protocol must also be provided in the manuscript.

## Dual use research of concern

Policy information about [dual use research of concern](#)

### Hazards

Could the accidental, deliberate or reckless misuse of agents or technologies generated in the work, or the application of information presented in the manuscript, pose a threat to:

No	Yes	
<input type="checkbox"/>	<input type="checkbox"/>	Public health
<input type="checkbox"/>	<input type="checkbox"/>	National security
<input type="checkbox"/>	<input type="checkbox"/>	Crops and/or livestock
<input type="checkbox"/>	<input type="checkbox"/>	Ecosystems
<input type="checkbox"/>	<input type="checkbox"/>	Any other significant area

## Experiments of concern

Does the work involve any of these experiments of concern:

- | No                       | Yes                      |   |
|--------------------------|--------------------------|---|
| <input type="checkbox"/> | <input type="checkbox"/> | Demonstrate how to render a vaccine ineffective                             |
| <input type="checkbox"/> | <input type="checkbox"/> | Confer resistance to therapeutically useful antibiotics or antiviral agents |
| <input type="checkbox"/> | <input type="checkbox"/> | Enhance the virulence of a pathogen or render a nonpathogen virulent        |
| <input type="checkbox"/> | <input type="checkbox"/> | Increase transmissibility of a pathogen                                     |
| <input type="checkbox"/> | <input type="checkbox"/> | Alter the host range of a pathogen  |
| <input type="checkbox"/> | <input type="checkbox"/> | Enable evasion of diagnostic/detection modalities                           |
| <input type="checkbox"/> | <input type="checkbox"/> | Enable the weaponization of a biological agent or toxin                     |
| <input type="checkbox"/> | <input type="checkbox"/> | Any other potentially harmful combination of experiments and agents         |

## ChIP-seq

### Data deposition

- Confirm that both raw and final processed data have been deposited in a public database such as [GEO](#).
- Confirm that you have deposited or provided access to graph files (e.g. BED files) for the called peaks.

Data access links

*May remain private before publication.*

*For "Initial submission" or "Revised version" documents, provide reviewer access links. For your "Final submission" document, provide a link to the deposited data.*

Files in database submission

*Provide a list of all files available in the database submission.*

Genome browser session

(e.g. [UCSC](#))

*Provide a link to an anonymized genome browser session for "Initial submission" and "Revised version" documents only, to enable peer review. Write "no longer applicable" for "Final submission" documents.*

### Methodology

Replicates

*Describe the experimental replicates, specifying number, type and replicate agreement.*

Sequencing depth

*Describe the sequencing depth for each experiment, providing the total number of reads, uniquely mapped reads, length of reads and whether they were paired- or single-end.*

Antibodies

*Describe the antibodies used for the ChIP-seq experiments; as applicable, provide supplier name, catalog number, clone name, and lot number.*

Peak calling parameters

*Specify the command line program and parameters used for read mapping and peak calling, including the ChIP, control and index files used.*

Data quality

*Describe the methods used to ensure data quality in full detail, including how many peaks are at FDR 5% and above 5-fold enrichment.*

Software

*Describe the software used to collect and analyze the ChIP-seq data. For custom code that has been deposited into a community repository, provide accession details.*

## Flow Cytometry

### Plots

Confirm that:

- The axis labels state the marker and fluorochrome used (e.g. CD4-FITC).
- The axis scales are clearly visible. Include numbers along axes only for bottom left plot of group (a 'group' is an analysis of identical markers).
- All plots are contour plots with outliers or pseudocolor plots.
- A numerical value for number of cells or percentage (with statistics) is provided.

### Methodology

Sample preparation

To prepare a single cell suspension of mouse skin, fat was removed from the overlying skin in PBS. Then the skin was incubated in collagenase type I (2 mg/ml in PBS) at 37°C for 75 min. After digestion, the skin was minced in RPMI/10% FBS, filtered through a 70- $\mu$ M cell strainer, and centrifuged at 300g for 7 min. Then the pellet was resuspended in RPMI/10% FBS, filtered through a 70- $\mu$ M cell strainer, and centrifuged at 300g for 7 min. Skin-draining lymph nodes were pooled, minced in RPMI/10% FBS, filtered through a 70- $\mu$ M cell strainer, and centrifuged at 300g for 7 min. The spleen was minced upon a 70-

$\mu$ M cell strainer, and the dissected pellets were incubated with RBC lysis buffer at RT for 5 min. All single cell suspensions were additionally processed for the indicated analyses. Peripheral blood mononuclear cells (PBMCs) were isolated from whole human blood by standard Ficoll-Paque (GE Healthcare) density gradient centrifugation. Purified lymphocytes were cryopreserved until use.

Instrument

Data were collected using BD FACS LSR II.

Software

Data from flow cytometry were analyzed with FlowJo™v.10.7.1 software for Windows.

Cell population abundance

Cell population abundance was reported as a proportion of a specific population (% of CD8+, etc).

Gating strategy

For all the experiments, single cells were gated on a forward scatter height vs. forward scatter area plot. Lymphocytes were gated on forward vs. side scatter plot based on their size and granularity. To exclude dead cells and non-T cells, LIVE/DEAD Fixable Dead Cell reactive dye+, CD14+, and CD19+ cells were gated out. T cells were gated with CD3 and CD8 gating.

Tick this box to confirm that a figure exemplifying the gating strategy is provided in the Supplementary Information.

## Magnetic resonance imaging

### Experimental design

Design type

*Indicate task or resting state; event-related or block design.*

Design specifications

*Specify the number of blocks, trials or experimental units per session and/or subject, and specify the length of each trial or block (if trials are blocked) and interval between trials.*

Behavioral performance measures

*State number and/or type of variables recorded (e.g. correct button press, response time) and what statistics were used to establish that the subjects were performing the task as expected (e.g. mean, range, and/or standard deviation across subjects).*

### Acquisition

Imaging type(s)

*Specify: functional, structural, diffusion, perfusion.*

Field strength

*Specify in Tesla*

Sequence &amp; imaging parameters

*Specify the pulse sequence type (gradient echo, spin echo, etc.), imaging type (EPI, spiral, etc.), field of view, matrix size, slice thickness, orientation and TE/TR/flip angle.*

Area of acquisition

*State whether a whole brain scan was used OR define the area of acquisition, describing how the region was determined.*

Diffusion MRI

 Used

 Not used

### Preprocessing

Preprocessing software

*Provide detail on software version and revision number and on specific parameters (model/functions, brain extraction, segmentation, smoothing kernel size, etc.).*

Normalization

*If data were normalized/standardized, describe the approach(es): specify linear or non-linear and define image types used for transformation OR indicate that data were not normalized and explain rationale for lack of normalization.*

Normalization template

*Describe the template used for normalization/transformation, specifying subject space or group standardized space (e.g. original Talairach, MNI305, ICBM152) OR indicate that the data were not normalized.*

Noise and artifact removal

*Describe your procedure(s) for artifact and structured noise removal, specifying motion parameters, tissue signals and physiological signals (heart rate, respiration).*

Volume censoring

*Define your software and/or method and criteria for volume censoring, and state the extent of such censoring.*

### Statistical modeling & inference

Model type and settings

*Specify type (mass univariate, multivariate, RSA, predictive, etc.) and describe essential details of the model at the first and second levels (e.g. fixed, random or mixed effects; drift or auto-correlation).*

Effect(s) tested

*Define precise effect in terms of the task or stimulus conditions instead of psychological concepts and indicate whether ANOVA or factorial designs were used.*

Specify type of analysis:  Whole brain  ROI-based  Both

Statistic type for inference  
(See [Eklund et al. 2016](#))

*Specify voxel-wise or cluster-wise and report all relevant parameters for cluster-wise methods.*

## Models &amp; analysis

n/a | Involved in the study

  Functional and/or effective connectivity  Graph analysis  Multivariate modeling or predictive analysis

Functional and/or effective connectivity

*Report the measures of dependence used and the model details (e.g. Pearson correlation, partial correlation, mutual information).*

Graph analysis

*Report the dependent variable and connectivity measure, specifying weighted graph or binarized graph, subject- or group-level, and the global and/or node summaries used (e.g. clustering coefficient, efficiency, etc.).*

Multivariate modeling and predictive analysis

*Specify independent variables, features extraction and dimension reduction, model, training and evaluation metrics.*